Automatica 171 (2025) 111935

Contents lists available at ScienceDirect

Automatica

journal homepage: www.elsevier.com/locate/automatica

Linear formation control of multi-agent systems☆

Xiaozhen Zhang [a,b], Qingkai Yang [a,b,*], Fan Xiao [c], Hao Fang [a,b], Jie Chen [b,d]

[a] School of Automation, Beijing Institute of Technology, Beijing 100081, China
[b] National Key Laboratory of Autonomous Intelligent Unmanned Systems, Beijing 100081, China
[c] Institute of Remote Sensing Satellite, China Aerospace Science and Technology, Beijing 100094, China
[d] Department of Control Science and Engineering, Tongji University, Shanghai 201804, China

ARTICLE INFO

Article history:
Received 3 November 2023
Received in revised form 5 May 2024
Accepted 25 July 2024
Available online xxxx

Keywords:
Formation control
Linear transformation
Multi-agent systems
Distributed estimation
Affine formation control

ABSTRACT

This paper proposes a new distributed leader–follower control architecture, termed linear formation control, to realize formation variations. The objective is to navigate a group of agents to reach a specific target formation, which is a linear transformation of the pre-defined nominal configuration, whose dimension can be higher than agents' coordinates. The proposed architecture enables the formation to adjust through arbitrary linear transformations to accommodate the environment, offering a diverse range of feasible formations. First, we introduce the concept of "linear localizability" that leaders can uniquely determine the target formation. Then, using the pre-defined stress matrix, we propose a linear formation control method, which can be regarded as an extension of recent affine formation control approaches. Next, in the situation where the stress matrix is unavailable, distributed estimators are designed to obtain accurate linear formation parameters. We propose an estimation-driven linear formation control method using the graph Laplacian matrix. Finally, simulations are conducted to verify the effectiveness of the proposed linear formation control schemes.

1. Introduction

Formation control represents a fundamental cooperative behavior of multi-agent systems, demonstrating its successful applications in various scenarios, such as aerial surveillance (Beard, McLain, Nelson, Kingston, & Johanson, 2006), cooperative transportation (Zhang, Zhang, & Huang, 2024; Zhang et al., 2021), agricultural operations (Guillet, Lenain, Thuilot, & Rousseau, 2017), and space missions (Gill, Sundaramoorthy, Bouwmeester, Zandbergen, & Reinhard, 2013). However, due to the changes of the ambient environment in diverse cooperative tasks, it is typically necessary for formations to vary accordingly.

In the last decade, there have been growing interests in the study of formation scaling and rotation. It is shown a pair of agents is sufficient to determine the formation scaling size (see, e.g., Coogan and Arcak (2012), Han, Wang, Lin, and Zheng (2016), Liu, Ma, Zhang, and Huang (2023), Yang, Cao, Sun, Fang, and Chen (2018), Zhao and Zelazo (2017)) and rotation (see, e.g., Buckley & Egerstedt, 2021; Chen, Yang, Shi, Li, & Feroskhan, 2022). The desired scaling size can be estimated by using relative displacement measurements (Coogan & Arcak, 2012; Han et al., 2016; Liu et al., 2023; Yang et al., 2018). With the fact of bearing invariant in formation scaling, a bearing-based control method is proposed in Zhao and Zelazo (2017) for formation scaling maneuver. The scaling control strategy has also been applied to practical robotic systems in Lu, Wen, Shen, and Zhang (2021), Zhang, Wang, Wang, and Tian (2023), where adaptive neural network techniques are utilized to deal with the uncertainties of robot dynamics. By constructing triangulations in planar formation problems, bearing-only formation control schemes are proposed to achieve the desired rotation and scaling size in Buckley and Egerstedt (2021), Chen et al. (2022). Besides, when relative angles can only be obtained in agents' local coordinate frames, angle rigidity is introduced as an extension of bearing rigidity in Chen, Cao, and Li (2021), where the corresponding angle-only formation control scheme is also given, but as addressed in Chen and Sun (2023), only almost global stability can be is guaranteed in usually. Additionally, a coordinate-free formation control method that enables scaling and rotation is proposed in Mehdifar, Bechlioulis, Hendrickx, and Dimarogonas (2023), where the desired formation is constrained by variables of bearing and ratio of the distances in bipolar coordinates. Formation rotation and scaling have also been achieved in Garcia de Marina, Cao, and Jayawardhana (2015), Garcia De Marina, Jayawardhana, and

☆ The material in this paper was not presented at any conference. This paper was recommended for publication in revised form by Associate Editor Charalampos Bechlioulis under the direction of Editor Christos G. Cassandras.

* Corresponding author at: School of Automation, Beijing Institute of Technology, Beijing 100081, China.
E-mail addresses: jiaozhen@mail.nwpu.edu.cn (X. Zhang), qingkai.yang@bit.edu.cn (Q. Yang), xiaofanbit22@163.com (F. Xiao), fangh@bit.edu.cn (H. Fang), chenjie@bit.edu.cn (J. Chen).

https://doi.org/10.1016/j.automatica.2024.111935

Cao (2016) through the utilization of inconsistent distance measurements. For high-order nonholonomic systems, a distributed planar formation control method is presented to stabilize the formation with the desired scale size and any rotation up to $\pm 90^\circ$ in Fathian, Safaoui, Summers, and Gans (2021), where matrix-weighted edges are used to represent interactive relationships among agents. Furthermore, scaling and rotation behaviors can also be attained by manipulating the complex-Laplacian matrix associated with the underlying graph (see, e.g., Garcia de Marina, 2021; Motoyama & Cai, 2019), but it is worth noting that the modified matrix has to be computed centrally. To address the challenge of designing formation sizes in dynamic environments, online cooperative decision-making methods are proposed in Zhang, Lv, Lu, and Yang (2022), Zhang, Yang, Lyu, Zhao, and Fang (2024) to manage formation scaling parameters. Within this method, distributed average tracking filters are designed to guarantee consensus among local scaling parameters. It is noticed that scaling and rotation are two specific types of affine transformation motions. A general affine transformation encompasses a broader range of formation variations, including translation, scaling, rotation, shear, reflection, and their combinations.

Recently, the affine formation control approach has gained intense attention. In Lin, Wang, Chen, Fu, and Han (2016), the necessary and sufficient conditions of affine formation realization and stabilization have been provided for both directed and undirected graphs. The problem of time-varying affine formation maneuver control is explored in Zhao (2018). However, in the designed formation tracking controllers, inputs from neighboring agents are required. This controller is further extended to triple integrators (Onuoha, Tnunay, Li, & Ding, 2019). As an extreme case where only one agent is aware of the formation scaling size, an estimation-based control method is presented in Yang, Sun, Cao, Fang, and Chen (2019), relying only on relative positions to achieve the desired formation pattern. This method is further developed in Yang, Fang, Cao, and Chen (2022), where the desired rotation parameter can also be estimated. In addition to these studies, extensive research has been conducted on affine formation control. In Yang, Xiao, and Chen (2021), the affine formation problem within the special Euclidean space is studied, and the controller is directly tailored to the corresponding Lie algebra. To further improve convergence performance, various approaches such as finite-time, fixed-time, and prescribed-time affine formation control methods are studied in Lin, Lin, Sun, and Anderson (2022), Gao, Liu, Zhou, Zhao, and Huang (2022), and Wang, Ding, Wang, Liang, and Hu (2021), respectively. For broader applicability, affine formation control for general linear, high-order, time-delay, and heterogeneous systems are also explored in Onuoha, Tnunay, Wang, and Ding (2020), Xu, Zhao, Luo, and You (2020), Wang, Ding, Wang, Zuo, and Ding (2023), and Xu, Luo, Li, You, and Duan (2019), respectively. In addition, to optimize communication resource usage within physical robotic systems, event-triggered mechanisms are discussed for affine formation control schemes in Zhou, Huang, Mao, Zhu, and Su (2022), Zhu, Huang, Lu, Li, and Su (2023).

Although the transformation of formations from scaling and rotation to the affine manner has been studied, it is evident that these variations essentially can be represented by linear transformations. In pursuit of more diverse formation possibilities, this paper proposes a comprehensive architecture for general linear formation control of multi-agent systems. The principal objective of the linear formation control architecture is to realize the maneuvering of a group of agents toward a specified target formation, which is a linear transformation of the pre-defined nominal configuration. It is important to note that the dimension of this nominal configuration can be higher than agents' workspace. We proposed two sets of topological necessary and sufficient conditions for achieving "linear localizability"—a concept means that leaders can uniquely determine the target formation. These two sets of conditions provide the internal relations between the pre-defined stress matrix and desired target formations, and connect leaders' target formation with linear formation transformation parameters. Leveraging the above-mentioned properties, a stress matrix-based linear formation control method is proposed for realizing the target formation. Subsequently, a distributed estimator is devised to obtain the precise transformation parameters proceeding to achieving the desired formation shape.

The main contributions of this paper are given as follows:

(1) We propose a new distributed leader–follower formation control architecture, which we refer to as linear formation control. The proposed architecture empowers a group of agents to formation maneuver via arbitrary linear transformations with a rectangular matrix. This allows more feasible formations for adapting to different environments.
(2) We propose and prove the sufficient and necessary conditions that leaders can uniquely determine the target formation, termed "linear localizability".
(3) With a pre-defined stress matrix, we propose a linear formation control scheme for formation tracking which can be regarded as an extension of recent affine formation control approaches (Lin et al., 2016; Yang et al., 2019; Zhao, 2018). When the nominal formation is exactly lying in the same dimensional space as the agents' workspace, our proposed control scheme degenerates to the affine formation control method. In particular, we expand the formation transformation matrix from a square matrix specialized in the affine formation control method to a general rectangular matrix.
(4) When the stress matrix is unavailable, a distributed estimator is proposed to obtain the precise linear formation parameters for achieving target formation tracking.

The rest of this paper is organized as follows. First, some preliminaries are given in Section 2. Then, the linear formation problem is addressed in Section 3. In Section 4, the necessary and sufficient conditions for linear localizability are presented. We further proposed two distributed linear formation control methods using the stress matrix and distributed estimation, respectively. Next, simulations are given to verify the effectiveness of the proposed linear formation control schemes in Section 5. Finally, Section 6 concludes this article.

2. Preliminaries

This section presents some notations and preliminary results that will be used in this paper.

2.1. Notations

Let $\otimes$ denote the Kronecker product. For a matrix $\mathbf{F} \in \mathbb{R}^{m\times n}$, $\mathbf{F}^+ \in \mathbb{R}^{n\times m}$, and rank $(\mathbf{F})$ denote its Moore–Penrose inverse,[1] and rank, respectively. vec$(\cdot)$ is the vector obtained by stacking all columns of a matrix. The vectorization of $\mathbf{F}$ is represented by $\text{vec}(\mathbf{F}) = \left[\boldsymbol{f}_1^{\mathrm{T}}, \ldots, \boldsymbol{f}_n^{\mathrm{T}}\right]^{\mathrm{T}}$, where $\boldsymbol{f}_i$ denotes the ith column of $\mathbf{F}$. We use null$(\cdot)$ and col$(\cdot)$ to represent the null and column space of a matrix, respectively. dim$(\cdot)$ is the dimension of a linear space. Denote the identity matrix with dimension n by $\mathbf{I}_n$. We use diag $(\mathbf{D}_1, \ldots, \mathbf{D}_n)$ to represent the block-diagonal matrix with each diagonal block being $\mathbf{D}_i$. For a set $\mathcal{V}$, $|\mathcal{V}|$ denotes the number of elements in $\mathcal{V}$.

[1] For a matrix $\mathbf{F} \in \mathbb{R}^{m\times n}$, if rank$(\mathbf{F}) = m$, it has $\mathbf{F}\mathbf{F}^+ = \mathbf{I}_m$. If rank$(\mathbf{F}^{\mathrm{T}}) = n$, it has $\mathbf{F}^+\mathbf{F} = \mathbf{I}_n$ (Horn & Johnson, 2012).

2.2. Graph Theory (Godsil & Royle, 2001; Opsahl & Panzarasa, 2009) and Graph Rigidity Theory (Alfakih, 2011)

An undirected graph $\mathcal{G}$ is a pair $(\mathcal{V}, \mathcal{E})$, where $\mathcal{V} = \{v_1, \ldots, v_n\}$ is a non-empty finite set of nodes and $\mathcal{E} \subseteq \mathcal{V} \times \mathcal{V}$ is a set of ordered pairs of nodes, called edges. An edge (v_j, v_i) represents the connected path from node v_j to node v_i.

The Laplacian matrix $\mathcal{L} \in \mathbb{R}^{n\times n}$ of $\mathcal{G}$ is defined as

$$[\mathcal{L}]_{ij} = \begin{cases} -[\mathcal{A}]_{ij} & i \neq j \\ \sum_{k\in\mathcal{N}_i}[\mathcal{A}]_{ik} & i = j \end{cases},$$

where $\mathcal{N}_i = \{j \in \mathcal{V} : (v_j, v_i) \in \mathcal{E}\}$ is a set containing all neighbors of node v_i; $\mathcal{A} \in \mathbb{R}^{n\times n}$ is the adjacency matrix of $\mathcal{G}$, where $[\mathcal{A}]_{ii} = 0$, $[\mathcal{A}]_{ij} = 1$ for $(v_j, v_i) \in \mathcal{E}$ and $[\mathcal{A}]_{ij} = 0$ otherwise. For an undirected connected graph, the Laplacian matrix is positive semi-definite and has only one zero eigenvalue.

The incidence matrix $\mathcal{H} = [h_{ik}] \in \mathbb{R}^{|\mathcal{V}|\times|\mathcal{E}|}$ is defined as

$$h_{ik} = \begin{cases} 1 & \text{if } v_i \text{ is the head node of } k\text{th edge} \\ -1 & \text{if } v_i \text{ is the tail node of } k\text{th edge} \\ 0 & \text{otherwise} \end{cases}.$$

The incidence matrix and Laplacian matrix satisfy $\mathcal{L} = \mathcal{H}\mathcal{H}^{\mathrm{T}}$.

If the nodes' coordinates in $\mathbb{R}^f$ are $\boldsymbol{q} = \begin{bmatrix}\boldsymbol{q}_1^{\mathrm{T}} & \cdots & \boldsymbol{q}_n^{\mathrm{T}}\end{bmatrix}^{\mathrm{T}} \in \mathbb{R}^{nf}$, $\boldsymbol{q}$ is referred as a configuration. Here we can define a framework by the configuration $\boldsymbol{q}$ and the graph $\mathcal{G}$.

Definition 1 (*Framework (Lin et al., 2016)*)**.** A framework $(\mathcal{G}, \boldsymbol{q})$ in $\mathbb{R}^f$ is the undirected graph $\mathcal{G}$ equipped with the configuration $\boldsymbol{q}$.

An equilibrium stress of the framework $(\mathcal{G}, \boldsymbol{q})$ is a set of scalars $\{\omega_{ij}\}_{i,j\in\mathcal{E}}$, $\omega_{ij} \in \mathbb{R}$, such that

$$\sum_{j\in\mathcal{N}_i} \omega_{ij}(\boldsymbol{q}_i - \boldsymbol{q}_j) = \boldsymbol{0}_f, \qquad \forall i \in \mathcal{V}, \tag{1}$$

where $\omega_{ij}(\boldsymbol{q}_i - \boldsymbol{q}_j)$ can be regarded as the force exerted by the edge (v_i, v_j) on node v_i. This force is called a tension when $\omega_{ij} > 0$, and a compression when $\omega_{ij} < 0$. Thus, Eq. (1) represents that the forces applied on v_i by $\{v_j\}_{j\in\mathcal{N}_i}$ are balanced. Eq. (1) can also be rewritten into the following compact form:

$$(\Omega \otimes \mathbf{I}_f)\boldsymbol{q} = \boldsymbol{0}_{nf},$$

where $\Omega \in \mathbb{R}^{n\times n}$ is called the stress matrix given by

$$[\Omega]_{ij} = \begin{cases} 0 & (v_j, v_i) \notin \mathcal{E} \\ -\omega_{ij} & (v_j, v_i) \in \mathcal{E} \\ \sum_{k\in\mathcal{N}_i}\omega_{ik} & i = j \end{cases}.$$

It is noted that the stress matrix has a similar structure to the Laplacian matrix. However, one difference is that the weight for an edge in the stress matrix can be positive, negative, or zero. This leads to the fact that the stress matrix is not necessarily positive semi-definite, even if the corresponding graph is undirected connected.

2.3. Linear transformation (Lay, Lay, & McDonald, 2014)

2.3.1. Linear transformation

The linear transformation $\mathcal{W} : \mathbb{R}^{n_1} \to \mathbb{R}^{n_2}$ is a function (or mapping) from the vector space $\mathbb{R}^{n_1}$ to $\mathbb{R}^{n_2}$. A linear transformation can be expressed in the following form:

$$\mathcal{W}(\boldsymbol{x}) = \mathbf{A}\boldsymbol{x},$$

where $\boldsymbol{x} \in \mathbb{R}^{n_1}$; $\mathcal{W}(\boldsymbol{x}) \in \mathbb{R}^{n_2}$ is the image of $\boldsymbol{x}$; $\mathbf{A} \in \mathbb{R}^{n_2\times n_1}$ is a rectangular linear transformation matrix. The linear transformation satisfies the following two properties:

- *Additivity:* $\mathcal{W}(\boldsymbol{y}) + \mathcal{W}(\boldsymbol{z}) = \mathcal{W}(\boldsymbol{y} + \boldsymbol{z})$,
- *Homogeneity:* $c\mathcal{W}(\boldsymbol{y}) = \mathcal{W}(c\boldsymbol{y})$,

where $\boldsymbol{y}, \boldsymbol{z} \in \mathbb{R}^{n_1}$, $c \in \mathbb{R}$.

2.3.2. Linear span

For a set of N vectors $\{\boldsymbol{x}_i\}_{i=1}^N$ in $\mathbb{R}^{n_1}$, the linear span $\mathcal{S}$ of those vectors is the set of all finite linear combinations of elements (vectors), such that

$$\mathcal{S} = \left\{\sum_{i=1}^N a_i\boldsymbol{x}_i : a_i \in \mathbb{R}\right\}.$$

The dimension of the obtained linear space $\mathcal{S}$ is defined as the dimension of the linear span. If the dimension of the linear span is n_2, then we can say that the vectors $\{\boldsymbol{x}_i\}_{i=1}^N$ linearly span $\mathbb{R}^{n_2}$.

2.4. Affine transformation (Artin, 1988; Li, Wang, & Wang, 2010; Tofallis, Gass, & Harris, 2013)

In $\mathbb{R}^m$, affine transformation $\mathcal{A} : \mathbb{R}^m \to \mathbb{R}^m$ is a shifted linear transformation. For $\boldsymbol{x} \in \mathbb{R}^m$, $\mathcal{A}(\boldsymbol{x}) \in \mathbb{R}^m$ is the called the affine image of $\boldsymbol{x}$. An affine transformation can be expressed in the following form:

$$\mathcal{A}(\boldsymbol{x}) = \mathbf{A}\boldsymbol{x} + \boldsymbol{b},$$

where $\mathbf{A} \in \mathbb{R}^{m\times m}$ is a square linear transformation matrix; $\boldsymbol{b} \in \mathbb{R}^m$ is a translation vector.

The affine image can preserve some of the relationships of the original image, including the collinearity between points, parallelism, ratios of lengths of parallel line segments, and barycenters.

2.5. Solutions of a system of linear equations (Lay et al., 2014)

A system of linear equations about $\boldsymbol{x} \in \mathbb{R}^c$ can be written in the following form

$$\mathbf{A}\boldsymbol{x} = \boldsymbol{b}, \tag{2}$$

where $\mathbf{A} \in \mathbb{R}^{r\times c}$, $\boldsymbol{b} \in \mathbb{R}^r$. The solutions of the system of linear equations (2) are identified based on the rank conditions of $\mathbf{A}$ and $\boldsymbol{b}$, given by

(1) $\mathbf{A}\boldsymbol{x} = \boldsymbol{b}$ has only one solution, if $\operatorname{rank}\left(\begin{bmatrix}\mathbf{A} & \boldsymbol{b}\end{bmatrix}\right) = \operatorname{rank}(\mathbf{A}) = c$;
(2) $\mathbf{A}\boldsymbol{x} = \boldsymbol{b}$ has infinite solutions, if $\operatorname{rank}\left(\begin{bmatrix}\mathbf{A} & \boldsymbol{b}\end{bmatrix}\right) = \operatorname{rank}(\mathbf{A}) < c$;
(3) $\mathbf{A}\boldsymbol{x} = \boldsymbol{b}$ has no solution, if $\operatorname{rank}(\mathbf{A}) < \operatorname{rank}\left(\begin{bmatrix}\mathbf{A} & \boldsymbol{b}\end{bmatrix}\right)$.

3. Problem statement

Consider a group of n agents in $\mathbb{R}^d$, where $d \in \mathbb{N}^+$, $n \geq f + 1$, $f \geq d$, and $f \in \mathbb{N}^+$. The agents consist of n_l leaders and n_f followers. $\mathcal{V}$, $\mathcal{V}_l$, and $\mathcal{V}_f$ represent agent, leader and follower sets, respectively. It has $\mathcal{V}_l \cap \mathcal{V}_f = \varnothing$.

The group of n agents satisfies the following single-integrator dynamics:

$$\dot{\boldsymbol{p}}_i = \boldsymbol{u}_i, \qquad i = 1, \ldots, n. \tag{3}$$

where $\boldsymbol{u}_i \in \mathbb{R}^d$ is control input and $\boldsymbol{p}_i \in \mathbb{R}^d$ represents the position.

Some definitions are given before presenting the problem.

Definition 2 (*Nominal Configuration*)**.** The nominal configuration $\{\boldsymbol{r}_i\}_{i=1}^n$, $\boldsymbol{r}_i \in \mathbb{R}^f$ is a set of predefined vectors associated with each agent.

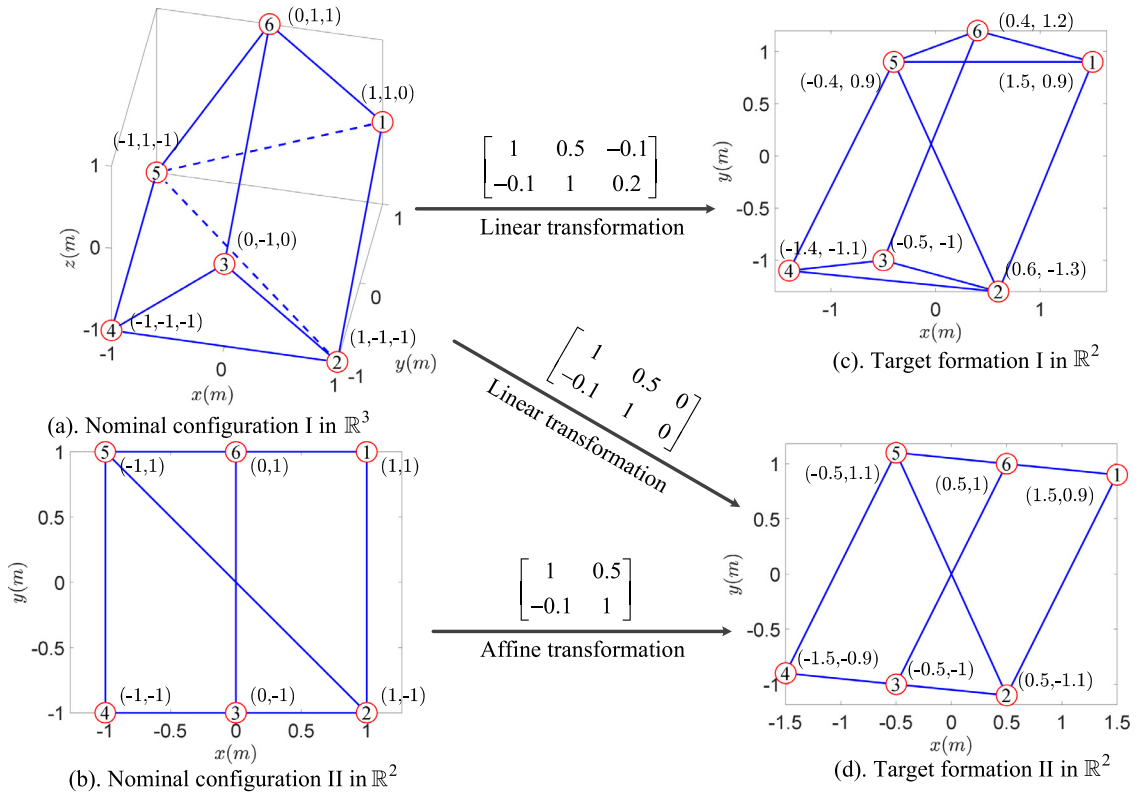

Fig. 1. An example of linear and affine formation transformations. Both target formations I and II in (c) and (d) can be obtained via linear transformations from the nominal configuration I in (a). However, there is no nominal configuration that can affinely transform into (c) and (d). It is because affine transformation is unable to destroy collinear relationships (see Section 2.4). For example, the nodes 2, 3 and 4 are collinear in (d), but non-collinear in (c). Further, note that the projection of the nominal configuration (a) on the *xOy* plane is exactly the nominal configuration (b). Therefore, all of the feasible formations, that are affinely transformed from the nominal configuration (b), can also be achieved by (a) with the last column of the linear transformation matrix zero. For example, the target formation (d) can be obtained from the nominal configuration of both (a) and (b) by properly linear and affine transformation, respectively.

Definition 3 (*Augmented Nominal Configuration*)**.**
$\bar{\boldsymbol{r}}_i = \begin{bmatrix} \boldsymbol{r}_i^{\mathrm{T}} & 1 \end{bmatrix}^{\mathrm{T}} \in \mathbb{R}^{f+1}$ is called the augmented nominal configuration.

Definition 4 (*Target Formation*)**.**
The target formation $\boldsymbol{p}_i^* \in \mathbb{R}^d$ is the desired position for the agents. It is a linear transformation of the augmented nominal configuration, expressed as

$$\boldsymbol{p}_i^* = \bar{\mathbf{A}}\bar{\boldsymbol{r}}_i = \mathbf{A}\boldsymbol{r}_i + \boldsymbol{b}, \tag{4}$$

where $\mathbf{A} \in \mathbb{R}^{d\times f}$ is a rectangular transformation matrix; $\boldsymbol{b} \in \mathbb{R}^d$ is a translation vector; $\bar{\mathbf{A}} = \begin{bmatrix} \mathbf{A} & \boldsymbol{b} \end{bmatrix} \in \mathbb{R}^{d\times(f+1)}$. $\mathbf{A}\boldsymbol{r}_i$ and $\boldsymbol{b}$ determine the geometric shape and translation movement of the target formation, respectively. f and d are the space dimensions in which the nominal configuration and target formation is defined, respectively. It satisfies $f \geq d$. All possible target formations constitute the image space of the linear transformation of $\bar{\mathbf{A}}$, defined as

$$\mathcal{T}(\bar{\boldsymbol{r}}) = \left\{\boldsymbol{p}^* \in \mathbb{R}^{dn} : \boldsymbol{p}^* = (\mathbf{I}_n \otimes \bar{\mathbf{A}})\bar{\boldsymbol{r}}\right\},$$

where

$$\boldsymbol{p}^* = \left[\left(\boldsymbol{p}_1^*\right)^{\mathrm{T}} \quad \cdots \quad \left(\boldsymbol{p}_n^*\right)^{\mathrm{T}}\right]^{\mathrm{T}},$$
$$\bar{\boldsymbol{r}} = \left[\bar{\boldsymbol{r}}_1^{\mathrm{T}} \quad \cdots \quad \bar{\boldsymbol{r}}_n^{\mathrm{T}}\right]^{T}.$$

Although the transformation described in (4) can also be written in the form of $\mathbf{A}\boldsymbol{r}_i + \boldsymbol{b}$, the linear part $\mathbf{A}$ still can be a rectangle matrix. Consequently, the transformation (4) is a linear transformation $\hat{\mathcal{T}}(\bar{\boldsymbol{r}}_i) : \mathbb{R}^{f+1} \to \mathbb{R}^d$, where $\hat{\mathcal{T}}(\bar{\boldsymbol{r}}_i) = \left\{\boldsymbol{p}_i^* \in \mathbb{R}^d, \boldsymbol{p}_i^* = \bar{\mathbf{A}}\bar{\boldsymbol{r}}_i\right\}$. The linear transformation $\hat{\mathcal{T}}(\bar{\boldsymbol{r}}_i)$ can map the nominal configuration of high-dimensional space to a specific target formation for maneuvering. Fig. 1 also illustrates that the proposed linear formation architecture can yield richer target formations compared to affine approaches (Lin et al., 2016; Zhao, 2018).

The graph $\mathcal{G}$ denotes the interactive relationship among agents. This paper designates the first n_l agents as leaders without loss of generality. The Laplacian matrix $\mathcal{L}$ and stress matrix Ω associated with the graph $\mathcal{G}$ are defined in the following forms that are consistent with the partition of leaders and followers:

$$\mathcal{L} = \begin{bmatrix} \mathcal{L}_{ll} & \mathcal{L}_{lf} \\ \mathcal{L}_{fl} & \mathcal{L}_{ff} \end{bmatrix}, \qquad \Omega = \begin{bmatrix} \Omega_{ll} & \Omega_{lf} \\ \Omega_{fl} & \Omega_{ff} \end{bmatrix}.$$

All followers forms the subgraph $\mathcal{G}_f$. The corresponding Laplacian matrix of $\mathcal{G}_f$ is defined as $\mathcal{L}_f$. $\mathcal{N}_i$ and $\mathcal{N}_{fi}$ denote the neighbor sets of the agent i in $\mathcal{G}$, and $\mathcal{G}_f$, respectively.

In this paper, all agents are aware of the nominal configuration, but only leaders know the desired target formation, which is parameterized by the augmented linear transformation matrix $\bar{\mathbf{A}}$. The primary objective is to develop control laws that enable all followers to converge to the specific target formation, i.e.,

$$\lim_{t\to\infty} \boldsymbol{p}_i(t) = \boldsymbol{p}_i^* = \bar{\mathbf{A}}\bar{\boldsymbol{r}}_i, i \in \mathcal{V}_f$$

We study the convergence under the following two scenarios.

Scenario 1: With a predefined stress matrix that connects the target formations of leaders and followers, the convergence is achieved by a stress matrix-driven control scheme.

Scenario 2: When the stress matrix is unavailable, the convergence is achieved by cooperatively identifying the linear transformation matrix $\mathbf{A}$.

4. Main results

Before providing the main results, the following Lemma introduces the algebraic transformations used in this paper.

Lemma 1. *For a matrix* $\mathbf{X} \in \mathbb{R}^{r\times c}$ *and vectors* $\{\boldsymbol{z}_i\}_{i=1,\dots,m}$, $\boldsymbol{z}_i \in \mathbb{R}^c$, *the following equation always holds*

$$(\mathbf{I}_m \otimes \mathbf{X})\,\boldsymbol{z} = (\mathbf{Z} \otimes \mathbf{I}_r)\,\mathrm{vec}\,(\mathbf{X})\,,$$

where $\mathbf{Z} = \begin{bmatrix}\boldsymbol{z}_1 & \dots & \boldsymbol{z}_m\end{bmatrix}^T$, $\boldsymbol{z} = \begin{bmatrix}\boldsymbol{z}_1^{\mathrm{T}} & \dots & \boldsymbol{z}_m^{\mathrm{T}}\end{bmatrix}^T$, $r, c, m \in \mathbb{N}^+$.

Proof. See Appendix A. □

Prior to the designing of control schemes, it is imperative to analyze the uniqueness of target formation. Now, we introduce a condition known as "linear localizability" that leaders can uniquely determine the target formation. The formal definition of linear localizability is given below.

Definition 5 (*Linear Localizability*)**.**
For the framework $(\mathcal{G}, \boldsymbol{r})$, linear localizability means that for any $\boldsymbol{p}^* = \begin{bmatrix}(\boldsymbol{p}_l^*)^T & (\boldsymbol{p}_f^*)^T\end{bmatrix}^T \in \mathcal{T}(\bar{\boldsymbol{r}})$, $\boldsymbol{p}_f^*$ can be uniquely determined by $\boldsymbol{p}_l^*$, where $\boldsymbol{p}_l^* \in \mathbb{R}^{dn_l}$ and $\boldsymbol{p}_f^* \in \mathbb{R}^{dn_f}$ are the target formations of leaders and followers, respectively.

If the nominal formation lie in the same Euclidean space as that of agents' coordinates (i.e., $f = d$), the concept of linear localizability is just the affine localizability introduced in Zhao (2018). However, higher dimensional nominal formations are allowed in linear localizability. It means linear localizability is the more general one. Here we introduce the following assumption and lemma, which is adapted from affine formation control approaches (Lin et al., 2016; Zhao, 2018).

Assumption 1. The framework $(\mathcal{G}, \boldsymbol{r})$ has a pre-defined positive semi-definite stress matrix $\boldsymbol{\Omega}$ satisfying $rank(\boldsymbol{\Omega}) = n - f - 1$.

Lemma 2. *For the framework* $(\mathcal{G}, \boldsymbol{r})$*, the following conditions (1)–(3) are equivalent. Furthermore, if the framework* $(\mathcal{G}, \boldsymbol{r})$ *satisfies Assumption 1, all of the following conditions are equivalent.*

(1) $\{\boldsymbol{r}_i\}_{i=1}^n$ *linearly span* $\mathbb{R}^f$.
(2) $n \geq f + 1$ *and* $\mathrm{rank}(\bar{\mathbf{R}}) = f + 1$, *where*

$$\bar{\mathbf{R}} = \begin{bmatrix}\bar{\mathbf{R}}_l & \bar{\mathbf{R}}_f\end{bmatrix} = \begin{bmatrix}\bar{\boldsymbol{r}}_1 & \dots & \bar{\boldsymbol{r}}_n\end{bmatrix}^T.$$

(3) $\dim(\mathcal{T}(\bar{\boldsymbol{r}})) = d(f + 1)$.
(4) $\mathcal{T}(\bar{\boldsymbol{r}}) = \mathrm{null}(\boldsymbol{\Omega} \otimes \mathbf{I}_d)$.

Proof. See Appendix B. □

Remark 1. Lemma 2 highlights that the stress matrix exhibits an internal relationship with target formations, thus rendering it a valuable tool in linear formation control. We can obtain the stress matrix satisfying Assumption 1 from centralized offline methods, including singular value decomposition (SVD) (Section 7.A in Zhao, 2018, Algorithm 1 in Yang, Sun, Cao, Fang, & Chen, 2017), or topological optimization (Xiao, Yang, Zhao, & Fang, 2022). In addition, if the framework $(\mathcal{G}, \boldsymbol{r})$ is *generic*,[2] the necessary and sufficient condition that satisfies Assumption 1 is that the framework $(\mathcal{G}, \boldsymbol{r})$ is *universally rigid*[3] (Theorem 2 in Alfakih, 2011).

We will elaborate two control schemes under the scenarios described in Section 3.

4.1. Stress matrix-based linear formation control

This subsection studies the convergence of followers' positions under **Scenario 1**. Only when the framework $(\mathcal{G}, \boldsymbol{r})$ is linearly localizable can leaders uniquely determine the desired positions of followers. Consequently, linear localizability stands as a fundamental prerequisite for the proposed linear formation control architecture. Following, we analyze the necessary and sufficient conditions for linear localizability.

Assumption 2. $\boldsymbol{r}_l$ linearly spans $\mathbb{R}^f$, where $\boldsymbol{r}_l = \begin{bmatrix}\boldsymbol{r}_1^{\mathrm{T}} & \dots & \boldsymbol{r}_{n_l}^{\mathrm{T}}\end{bmatrix}^{\mathrm{T}}$.

Theorem 1. *The framework* $(\mathcal{G}, \boldsymbol{r})$ *is linearly localizable if and only if Assumption 2 is satisfied. Furthermore,*

$$\boldsymbol{p}_f^* = (\bar{\mathbf{R}}_f \otimes \mathbf{I}_d)(\bar{\mathbf{R}}_l^+ \otimes \mathbf{I}_d)\boldsymbol{p}_l^*. \tag{5}$$

Proof. (Sufficiency) By invoking Lemma 1, it is considered that $\boldsymbol{p}_l^*$ has been determined by a linear transformation $\bar{\mathbf{A}}$, such that

$$\boldsymbol{p}_l^* = \left(\mathbf{I}_{n_l} \otimes \bar{\mathbf{A}}\right)\bar{\boldsymbol{r}}_l = (\bar{\mathbf{R}}_l \otimes \mathbf{I}_d)\mathrm{vec}(\bar{\mathbf{A}}). \tag{6}$$

where $\bar{\boldsymbol{r}}_l = \begin{bmatrix}\bar{\boldsymbol{r}}_1^{\mathrm{T}} & \dots & \bar{\boldsymbol{r}}_{n_l}^{\mathrm{T}}\end{bmatrix}^{\mathrm{T}}$. If $\boldsymbol{r}_l$ linearly span $\mathbb{R}^f$, according to Lemma 2, it can be derived that $\mathrm{rank}(\bar{\mathbf{R}}_l) = f + 1$ and $n_l \geq f + 1$. Then, $\mathrm{vec}(\bar{\mathbf{A}})$ can be uniquely obtained by

$$\mathrm{vec}(\bar{\mathbf{A}}) = (\bar{\mathbf{R}}_l^+ \otimes \mathbf{I}_d)\boldsymbol{p}_l^*.$$

Then, by using the above equality, followers' target position can be uniquely computed by

$$\begin{aligned}\boldsymbol{p}_f^* = \left(\mathbf{I}_{n_f} \otimes \bar{\mathbf{A}}\right)\bar{\boldsymbol{r}}_f &= (\bar{\mathbf{R}}_f \otimes \mathbf{I}_d)\mathrm{vec}(\bar{\mathbf{A}}) \\ &= (\bar{\mathbf{R}}_f \otimes \mathbf{I}_d)(\bar{\mathbf{R}}_l^+ \otimes \mathbf{I}_d)\boldsymbol{p}_l^*\end{aligned}$$

where $\bar{\boldsymbol{r}}_f = \begin{bmatrix}\bar{\boldsymbol{r}}_{n_l+1}^{\mathrm{T}} & \dots & \bar{\boldsymbol{r}}_n^{\mathrm{T}}\end{bmatrix}^T$. The linear localizability is proved.

(Necessity) In view of Section 2.5, if $\boldsymbol{r}_l$ do not linearly span $\mathbb{R}^f$, $\mathrm{rank}(\bar{\mathbf{R}}_l) < f + 1$, which does not satisfy the rank conditions for the system of linear equations (6) having the unique solution about $\mathrm{vec}(\bar{\mathbf{A}})$. Hence, $\mathrm{vec}(\mathbf{A})$ cannot be located, nor does $\boldsymbol{p}_f^*$. ■

Form Theorem 1, we know that $\boldsymbol{p}_f^*$ can be uniquely determined by $\boldsymbol{p}_l^*$ through (5). Then, the relationship between $\boldsymbol{\Omega}$ and $\boldsymbol{p}^*$ will be addressed in the following theorem.

Theorem 2. *Under Assumptions 1 and 2, followers' target formation* $\boldsymbol{p}_f^*$ *can be uniquely represented by (7) if and only if* $\boldsymbol{\Omega}_{ff}$ *is nonsingular.*

$$\boldsymbol{p}_f^* = -(\boldsymbol{\Omega}_{ff}^{-1}\boldsymbol{\Omega}_{fl} \otimes \mathbf{I}_d)\boldsymbol{p}_l^*. \tag{7}$$

Proof. (Sufficiency) In view of Lemma 2, it is also known that $\boldsymbol{p}^* \in \mathcal{T}(\bar{\boldsymbol{r}}) = \mathrm{null}(\boldsymbol{\Omega} \otimes \mathbf{I}_d)$, which means

$$(\boldsymbol{\Omega}_{ff} \otimes \mathbf{I}_d)\boldsymbol{p}_f^* + (\boldsymbol{\Omega}_{fl} \otimes \mathbf{I}_d)\boldsymbol{p}_l^* = \mathbf{0}_{dn_f}. \tag{8}$$

Then, $\boldsymbol{p}_f^* = -(\boldsymbol{\Omega}_{ff}^{-1}\boldsymbol{\Omega}_{fl} \otimes \mathbf{I}_d)\boldsymbol{p}_l^*$ can be obtained. The relation (7) is true.

(Necessity) In view of Section 2.5, if $\boldsymbol{\Omega}_{ff}$ is singular, $\mathrm{rank}(\boldsymbol{\Omega}_{ff}) < n_f$, which does not satisfy the rank conditions for the system of linear equations (8) having the unique solution about $\boldsymbol{p}_f^*$. Hence, $\boldsymbol{p}_f^*$ cannot be uniquely represented by (7). ■

[2] A framework $(\mathcal{G}, \boldsymbol{r})$ is generic if all the coordinates of all the points of $\boldsymbol{r}$ are algebraically independent over the rationals. Intuitively speaking, for a generic configuration, there can be no symmetries in the configuration, no three nodes stay on the same line, and no three lines go through the same node (Connelly & Gortler, 2015).

[3] A framework is universally rigid if any framework in any dimension with the same graph and edge lengths in a Euclidean image of it (Oba & ichi Tanigawa, 2021).

Although Theorems 1 and 2 have similar expressions as that in Lin et al. (2016) and Zhao (2018), this paper leverages the conclusions of the solution structure of a system of linear equations to make the proofs more concise.

According to Theorem 2, we also know that Ω_{ff} is positive definite. Consequently, when working with a framework $(\mathcal{G}, \boldsymbol{r})$ that satisfies Assumptions 1 and 2, the following classic stress matrix-based control law (9) from (Zhao, 2018) can also be used for achieving the convergence of followers' positions in the proposed linear formation control architecture.

$$\boldsymbol{u}_i = -k_f \sum_{j\in\mathcal{N}_i} \omega_{ij}(\boldsymbol{p}_i - \boldsymbol{p}_j), \qquad i \in \mathcal{V}_f \tag{9}$$

where k_f is a positive gain.

Remark 2. In this subsection, we demonstrate that the proposed stress matrix-based linear formation control scheme represents a more general form of the affine formation control approach. When the nominal formation exactly lies in $\mathbb{R}^d$, i.e., $f = d$ ($\mathbf{A}$ becomes a square matrix), the proposed approach degenerates to the affine formation control method described in Zhao (2018).

4.2. Estimation-based linear formation control

This subsection studies the position convergence of followers when the stress matrix is unavailable (**Scenario 2**). Theorem 1 also shows that there exists an internal connection between leaders' formation and linear formation parameters. Consequently, we propose a distributed estimation-driven linear formation control method that can estimate the linear formation parameter $\bar{\mathbf{A}}$ by observing leaders' edges. Foremost, the displacement measurability is defined as follows:

Definition 6 (*Displacement Measurability*)**.**
In the graph $\mathcal{G}$, if there exists a triplet[4] $\tau_{ji,ki}$, we say the displacement corresponding to the edge (v_j, v_k) is measurable by agent i.

According to Definition 6, note that it is unnecessary to ensure the existence of edge (v_j, v_k) in $\mathcal{G}$. The followers who can measure leaders' edges form the set $\mathcal{V}_{f1}$, and the other followers consist of $\mathcal{V}_{f2}$. It satisfies $\mathcal{V}_f = \mathcal{V}_{f1} \cup \mathcal{V}_{f2}$, $\mathcal{V}_{f1} \cap \mathcal{V}_{f2} = \varnothing$, and $\mathcal{V}_{f1} \neq \varnothing$.

The following assumptions always hold in this subsection.

Assumption 3. The subgraph $\mathcal{G}_f$ is undirected and connected. Then, its corresponding Laplacian matrix $\mathcal{L}_f$ is positive semi-definite.

Assumption 4. In the nominal configuration $\{\boldsymbol{r}_i\}_{i=1}^n$, $\boldsymbol{r}_i \in \mathbb{R}^f$, all measurable displacements determined by triplets $\{\tau_{ji,ki}\}$ linearly span $\mathbb{R}^f$, i.e.,

$$\text{span}\{..., \boldsymbol{r}_{jk}, ...\} = \mathbb{R}^f, \quad \text{for all } \mathcal{G}_s(\tau_{ji,ki}) \subset \mathcal{G},$$

where $i \in \mathcal{V}_{f1}$; $j, k \in \mathcal{V}_l$; $\boldsymbol{r}_{jk} = \boldsymbol{r}_j - \boldsymbol{r}_k$.

To estimate the desired linear transformation $\boldsymbol{x}^* = \text{vec}(\mathbf{A}) \in \mathbb{R}^{df}$, we define that follower' estimation $\boldsymbol{x}_i$ satisfies the following dynamics

$$\dot{\boldsymbol{x}}_i = \boldsymbol{\mu}_i, \qquad i \in \mathcal{V}_f. \tag{10}$$

We propose the following estimators for followers:

$$\begin{aligned}\boldsymbol{\mu}_i = &-\alpha_1 \mathbf{M}_i^{\mathrm{T}}\left(\mathbf{M}_i\boldsymbol{x}_i - \boldsymbol{\xi}_i\right)\\ &-\alpha_2 \sum_{j\in\mathcal{N}_{fi}}\left(\boldsymbol{x}_i - \boldsymbol{x}_j\right), \qquad i \in \mathcal{V}_{f1}\end{aligned} \tag{11}$$

$$\boldsymbol{\mu}_i = -\alpha_2 \sum_{j\in\mathcal{N}_{fi}}\left(\boldsymbol{x}_i - \boldsymbol{x}_j\right), \qquad i \in \mathcal{V}_{f2} \tag{12}$$

with

$$\begin{aligned}
&\boldsymbol{\xi}_i = \begin{bmatrix}\cdots & \boldsymbol{p}_{jk}^{\mathrm{T}} & \cdots\end{bmatrix}^{\mathrm{T}}, \quad j,k \in \mathcal{V}_l \cap \mathcal{N}_i,\\
&\mathbf{M}_i = \begin{bmatrix}\cdots & \mathbf{Q}_{jk}^{\mathrm{T}} & \cdots\end{bmatrix}^{\mathrm{T}}, \quad j,k \in \mathcal{V}_l \cap \mathcal{N}_i,\\
&\mathbf{Q}_{jk} = \boldsymbol{r}_{jk}^{\mathrm{T}} \otimes \mathbf{I}_d,\\
&\boldsymbol{p}_{jk} = \boldsymbol{p}_j - \boldsymbol{p}_k,\\
&\boldsymbol{r}_{jk} = \boldsymbol{r}_j - \boldsymbol{r}_k,
\end{aligned}$$

where $\mathcal{N}_{fi}$ denote the neighbor sets of the agent i in the subgraph $\mathcal{G}_f$; α_1 and α_2 are positive gains; $\boldsymbol{\xi}_i \in \mathbb{R}^{d|\mathcal{N}_{fi}|}$ consists of all measurable leaders' edges determined by triplets $\{\tau_{ji,ki}\}_{j,k\in\mathcal{V}_l}$; $\mathbf{Q}_{jk} \in \mathbb{R}^{d\times d^2}$ represents the matrix form of nominal formation $\boldsymbol{r}_{jk}$; $\mathbf{M}_i \in \mathbb{R}^{d|\mathcal{N}_{fi}|\times d^2}$ consists of all measurable leaders' matrix form of nominal formations determined by triplets $\{\tau_{ji,ki}\}_{j,k\in\mathcal{V}_l}$.

In (11)–(12), the term $\mathbf{M}_i^{\mathrm{T}}\left(\mathbf{M}_i\boldsymbol{x}_i - \boldsymbol{\xi}_i\right)$ is designed to identify $\boldsymbol{x}^*$ using local measurements $\boldsymbol{\xi}_i$. It requires local estimation $\boldsymbol{x}_i$ to satisfy $\mathbf{M}_i\boldsymbol{x}_i = \boldsymbol{\xi}_i$. The term $\sum_{j\in\mathcal{N}_{fi}}\left(\boldsymbol{x}_i - \boldsymbol{x}_j\right)$ is designed to let local estimations $\{\boldsymbol{x}_i\}_{i\in\mathcal{V}_f}$ reach consensus.

The control law for followers is designed as follows:

$$\boldsymbol{u}_i = -\beta \sum_{j\in\mathcal{N}_i}\left(\boldsymbol{p}_{ij} - \mathbf{Q}_{ij}\boldsymbol{x}_i\right), \qquad i \in \mathcal{V}_f \tag{13}$$

where β denotes a positive gain; $\mathbf{Q}_{ij}\boldsymbol{x}_i$ represents locally recognized target formation based on ith follower's estimation $\boldsymbol{x}_i$.

Remark 3. The estimation-based method in Section 4.2 demonstrates the utility under a sparser topological graph compared to that in the stress matrix-based method described in Section 4.1, specifically omitting the need for Assumption 1. For example, according to Remark 1, a universally rigid generic framework must have an available stress matrix (Alfakih, 2011), and must be associated with a rigid graph.[5] Henneberg d-construction (Whiteley, 2004) can construct a rigid graph with minimal edges in $\mathbb{R}^d$. It requires d new edges for each vertex addition. Therefore, the resulting rigid graph will have more edges as the dimension of the embedded Euclidean space increases, i.e., the dimension of the nominal configuration increases. In contrast, the estimation-based method only requires an undirected and connected topology (as addressed in Assumption 3) regardless of the dimension of the embedded Euclidean space. As shown in Fig. 2, subfigures (a) and (b) are used for stress matrix-based and estimation-based methods, respectively. We can see there are significantly less edges in Fig. 2(b) than that in (a).

Remark 4. It is also noted that the stress matrix-based method in Section 4.1 can be used with arbitrarily oriented local coordinate frames, because it can be verified that $\boldsymbol{u}_i = -k_f \sum_{j\in\mathcal{N}_i} \omega_{ij} \boldsymbol{\Xi}_i(\boldsymbol{p}_i - \boldsymbol{p}_j)$ is (9) in the oriented coordinate frame with rotation matrix $\boldsymbol{\Xi}_i \in \mathbb{R}^{d\times d}$. The estimation-based method in Section 4.2 can only be implemented with aligned local coordinate frames. However, explicit communication is required in the estimation-based

[4] The triplet $\tau_{ji,ki}$ admits a subgraph $\mathcal{G}_s(\tau_{ji,ki})$ consisting of three nodes and two edges, such that $\mathcal{G}_s(\tau_{ji,ki}) = (\mathcal{V}_s(\tau_{ji,ki}), \mathcal{E}_s(\tau_{ji,ki})) \subset \mathcal{G}$, where $\mathcal{V}_s(\tau_{ji,ki}) = \{v_i, v_j, v_k\}$, $\mathcal{E}_s(\tau_{ji,ki}) = \{(v_j, v_i), (v_k, v_i)\}$.

[5] A universally rigid framework must be globally rigid (Oba & ichi Tanigawa, 2021). A globally rigid framework is associated with a rigid graph (Anderson, Yu, & Hendrickx, 2008).

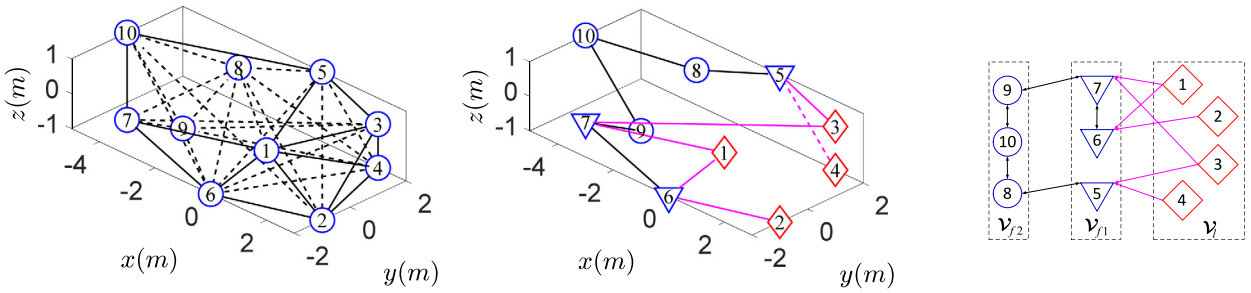

(a) A framework used in in Section 4.1, satisfying Assumptions 1-2. (b) A simplified framework used in Section 4.2, satisfying Assumptions 3. (c) Different agent sets and interactive relationship of (b).

Fig. 2. A comparison of topologies used in Sections 4.1 and 4.2. (a) is a framework satisfying Assumptions 1–2. It is computed by using the topology optimization proposed in Yang et al. (2017). We can see that agents 2, 4, and 6 all lie in the plane $z = 0$. Therefore, this framework is nongeneric. (a) can be used for the stress-based linear formation control described in Section 4.1. (b) is a simplified framework for the estimation-based linear formation control described in Section 4.2. (c) represents the agent sets of (b). In (b) and (c), there exist three triplets $\tau_{35,45}$, $\tau_{16,26}$, and $\tau_{17,37}$. Therefore, we can see $\mathcal{V}_l = \{1, 2, 3, 4\}$, $\mathcal{V}_{f1} = \{5, 6, 7\}$, $\mathcal{V}_{f2} = \{8, 9, 10\}$. $\mathcal{V}_{f1}$, $\mathcal{V}_{f2}$, and black edges constitute the subgraph $\mathcal{G}_f$. The pink edges denote the followers' measurements of the leaders' edges. We can see edges $(3, 4)$, $(1, 2)$, and $(1, 3)$ are measurable by followers 5, 6, and 7, respectively. (For interpretation of the references to color in this figure legend, the reader is referred to the web version of this article.)

method. This allows followers to align their local coordinate frames by an extra consensus protocol (Lee & Ahn, 2016).

Lemma 3. *Under Assumptions 3 and 4, the matrix $\mathbf{Y}+\bar{\mathcal{L}}_f$ is positive definite, where $\bar{\mathcal{L}}_f = \mathcal{L}_f \otimes \mathbf{I}_{df}$,*

$$\mathbf{Y} = \text{diag}([\mathbf{Y}_{n_l+1}, \mathbf{Y}_{n_l+2}, \dots, \mathbf{Y}_n]),$$
$$\mathbf{Y}_i = \begin{cases} \mathbf{M}_i^{\mathrm{T}}\mathbf{M}_i & i \in \mathcal{V}_{f1} \\ \mathbf{0}_{df\times df} & i \in \mathcal{V}_{f2} \end{cases}.$$

Proof. From the definition of $\mathbf{Y}_i$, one knows $\mathbf{Y}_i$ is a positive definite matrix when $i \in \mathcal{V}_{f1}$, and null matrix when $i \in \mathcal{V}_{f2}$. From the fact that $\mathcal{V}_{f1} \neq \varnothing$, it can be conducted that $\mathbf{Y}$ is positive semi-definite. In view of Assumption 3, it is obtained that $\bar{\mathcal{L}}_f$ is also positive semi-definite. Thus, in order to prove Lemma 3, it is sufficient to establish that $\mathbf{Y} + \bar{\mathcal{L}}_f$ is non-singular, which will be proved by assuming the contrary to obtain a contradiction.

Suppose there is a nonzero vector $\boldsymbol{\psi} \in \mathbb{R}^{n_f df}$ satisfying $\left(\mathbf{Y} + \bar{\mathcal{L}}_f\right)\boldsymbol{\psi} = \mathbf{0}_{n_f df}$. Then, it clearly has

$$\mathbf{Y}\boldsymbol{\psi} = \mathbf{0}_{n_f df},$$
$$\bar{\mathcal{L}}_f\boldsymbol{\psi} = \mathbf{0}_{n_f df}.$$

In view of $\bar{\mathcal{L}}_f\boldsymbol{\psi} = \mathbf{0}_{n_f df}$, $\boldsymbol{\psi}$ can be denoted by $\boldsymbol{\psi} = \mathbf{1}_{n_f} \otimes \boldsymbol{\theta}, \boldsymbol{\theta} \in \mathbb{R}^{df}$. Then, from $\mathbf{Y}\boldsymbol{\psi} = \mathbf{0}_{n_f df}$, we obtain $\mathbf{M}_i\boldsymbol{\theta} = \mathbf{0}_{df}$, $\forall i \in \mathcal{V}_{f1}$. For all followers belonging to $\mathcal{V}_{f1}$, they form the following system of linear equations:

$$\mathbf{M}_f\hat{\boldsymbol{\theta}} = \mathbf{0}_{|\mathcal{V}_{f1}|df}, \tag{14}$$

where

$$\mathbf{M}_f = \begin{bmatrix}\cdots & \mathbf{M}_i^{\mathrm{T}} & \cdots\end{bmatrix}^{\mathrm{T}}, \quad i \in \mathcal{V}_{f1}$$
$$\hat{\boldsymbol{\theta}} = \left(\mathbf{1}_{|\mathcal{V}_{f1}|} \otimes \boldsymbol{\theta}\right)$$

According to Assumption 4, the measurable leaders' edges linearly span $\mathbb{R}^f$ in the nominal configuration. Therefore, $\mathbf{M}_f$ is full rank, i.e., $\text{rank}\left(\mathbf{M}_f\right) = \text{rank}\left(\begin{bmatrix}\mathbf{M}_f & \mathbf{0}\end{bmatrix}\right) = df$. In view of Section 2.5, (14) has the unique solution about $\hat{\boldsymbol{\theta}}$ that satisfies $\boldsymbol{\theta} = \mathbf{0}_{df}$. It implies $\boldsymbol{\psi} = \mathbf{0}_{n_f df}$. This contradicts the hypothesis.

Hence, $\mathbf{Y} + \bar{\mathcal{L}}_f$ is non-singular, and thus positive definite. □

Theorem 3. *Consider leaders are equipped with appropriate tracking controller satisfying $\lim_{t\to\infty}\left[\boldsymbol{p}_l(t) - \boldsymbol{p}_l^*(t)\right] = \mathbf{0}_{dn_l}$. Under Assumptions 2, 3 and 4, for any $\alpha > 0$, the proposed estimator (11)–(12) can enforce all followers' local estimations with dynamics (10) to converge to the desired linear formation parameter, i.e.,*

$$\lim_{t\to\infty}\boldsymbol{x}_i(t) - \boldsymbol{x}^* = \mathbf{0}_{df}, \quad \forall i \in \mathcal{V}_f.$$

Proof. The position error is defined as

$$\tilde{\boldsymbol{p}}_i = \boldsymbol{p}_i - \boldsymbol{p}_i^* = \boldsymbol{p}_i - \bar{\mathbf{A}}\bar{\boldsymbol{r}}_i. \tag{15}$$

The estimation error is defined as

$$\boldsymbol{e}_i = \boldsymbol{x}_i - \boldsymbol{x}^*. \tag{16}$$

We define $\boldsymbol{\xi}_i^* = \mathbf{M}_i\boldsymbol{x}^*$. Then, according to (10), (11), and (16), the estimation error dynamics for follower $i \in \mathcal{V}_{f1}$ are given as below

$$\begin{aligned}\dot{\boldsymbol{e}}_i =& \dot{\boldsymbol{x}}_i \\ =& -\alpha_1\mathbf{M}_i^{\mathrm{T}}\left(\mathbf{M}_i\boldsymbol{x}_i - \boldsymbol{\xi}_i^* + \boldsymbol{\xi}_i^* - \boldsymbol{\xi}_i\right) \\ & - \alpha_2\sum_{j\in\mathcal{N}_{fi}}\left(\boldsymbol{x}_i - \boldsymbol{x}^* - \boldsymbol{x}_j + \boldsymbol{x}^*\right) \\ =& -\alpha_1\mathbf{M}_i^{\mathrm{T}}\mathbf{M}_i\left(\boldsymbol{x}_i - \boldsymbol{x}^*\right) + \alpha_1\mathbf{M}_i^{\mathrm{T}}\left(\boldsymbol{\xi}_i - \boldsymbol{\xi}_i^*\right) \\ & - \alpha_2\sum_{j\in\mathcal{N}_{fi}}\left(\boldsymbol{x}_i - \boldsymbol{x}^* - \boldsymbol{x}_j + \boldsymbol{x}^*\right) \\ =& -\alpha_1\mathbf{M}_i^{\mathrm{T}}\mathbf{M}_i\boldsymbol{e}_i + \alpha_1\mathbf{M}_i^{\mathrm{T}}\left(\boldsymbol{\xi}_i - \boldsymbol{\xi}_i^*\right) \\ & - \alpha_2\sum_{j\in\mathcal{N}_{fi}}\left(\boldsymbol{e}_i - \boldsymbol{e}_j\right).\end{aligned}$$

In view of (10), (12), and (16), the estimation error dynamics for follower $i \in \mathcal{V}_{f2}$ are obtained by

$$\begin{aligned}\dot{\boldsymbol{e}}_i =& -\alpha_2\sum_{j\in\mathcal{N}_{fi}}\left(\boldsymbol{x}_i - \boldsymbol{x}^* - \boldsymbol{x}_j + \boldsymbol{x}^*\right) \\ =& -\alpha_2\sum_{j\in\mathcal{N}_{fi}}\left(\boldsymbol{e}_i - \boldsymbol{e}_j\right).\end{aligned}$$

Thereby, the estimation error dynamics can be rewritten into the following matrix form:

$$\dot{\boldsymbol{e}} = -\alpha_1\mathbf{Y}\boldsymbol{e} - \alpha_1\mathbf{W}\bar{\mathcal{H}}_{lm}\tilde{\boldsymbol{p}} - \alpha_2\bar{\mathcal{L}}_f\boldsymbol{e},$$

where $\bar{\mathcal{H}}_{lm} = \left(\mathcal{H}_{lm}^{\mathrm{T}} \otimes \mathbf{I}_d\right)$; $\mathcal{H}_{lm}$ is the incidence matrix consisting of those measurable displacements of leaders; $\bar{\mathcal{L}}_f = \left(\mathcal{L}_f \otimes I_{df}\right)$, and

$$\mathbf{W} = diag\left(\left[\mathbf{W}_{n_l+1}, \mathbf{W}_{n_l+2}, \ldots, \mathbf{W}_n\right]\right),$$

$$\mathbf{W}_i = \begin{cases} \mathbf{M}_i^{\mathrm{T}} & i \in \mathcal{V}_{f1} \\ \mathbf{0}_{df \times df} & i \in \mathcal{V}_{f2} \end{cases}.$$

We consider the following Lyapunov function:

$$V_e = \frac{1}{2}\boldsymbol{e}^{\mathrm{T}}\boldsymbol{e},$$

whose derivative is

$$\begin{aligned} \dot{V}_e =& \boldsymbol{e}^{\mathrm{T}}\dot{\boldsymbol{e}} \\ =& -\alpha_1 \boldsymbol{e}^{\mathrm{T}}\mathbf{Y}\boldsymbol{e} - \alpha_1 \boldsymbol{e}^{\mathrm{T}}\mathbf{W}\bar{\mathcal{H}}_{lm}\tilde{\boldsymbol{p}} - \alpha_2 \boldsymbol{e}^{\mathrm{T}}\bar{\mathcal{L}}_f \boldsymbol{e}. \end{aligned}$$

From Lemma 3, we also know that $\mathbf{Y} + \bar{\mathcal{L}}_f$ is positive definite. Then, it gives

$$\begin{aligned} \dot{V}_e \leq & -2\min\{\alpha_1, \alpha_2\}\lambda_{\min}\left(\mathbf{Y} + \bar{\mathcal{L}}_f\right) V_e \\ & - \alpha_1 \boldsymbol{e}^{\mathrm{T}}\mathbf{W}\bar{\mathcal{H}}_{lm}\tilde{\boldsymbol{p}} \end{aligned},$$

In view of $\tilde{\boldsymbol{p}}_l \to \boldsymbol{0}$, $t \to \infty$, we know $\bar{\mathcal{H}}_{lm}\tilde{\boldsymbol{p}} \to \boldsymbol{0}$, which implies $\boldsymbol{e}^{\mathrm{T}}\mathbf{W}\bar{\mathcal{H}}_{lm}\tilde{\boldsymbol{p}} \to \boldsymbol{0}$, $t \to \infty$. Therefore, it has $\boldsymbol{e} \to \boldsymbol{0}$, $t \to \infty$. ■

Theorem 4. *Consider leaders are equipped with appropriate tracking controller satisfying* $\lim_{t\to\infty}\left[\boldsymbol{p}_l(t) - \boldsymbol{p}_l^*(t)\right] = \boldsymbol{0}_{dn_l}$. *Under Assumptions 2, 3 and 4, with the estimator (10)–(12), for any* $\beta > 0$, *the estimation-based formation control law (13) can enforce all followers with dynamics (3) to converge to the target formation, i.e.,*

$$\lim_{t\to\infty} \boldsymbol{p}_i(t) - \boldsymbol{p}_i^* = \boldsymbol{0}_d, \qquad i \in \mathcal{V}_f$$

Proof. In view of (3), (13), and (15), followers' position error dynamics are given by

$$\begin{aligned} \dot{\tilde{\boldsymbol{p}}}_i =& \boldsymbol{u}_i \\ =& -\beta\sum_{j\in\mathcal{N}_i}\left(\boldsymbol{p}_{ij} - \mathbf{Q}_{ij}\boldsymbol{x}_i\right) \\ =& -\beta\sum_{j\in\mathcal{N}_i}\left(\boldsymbol{p}_{ij} - \mathbf{Q}_{ij}\boldsymbol{x} + \mathbf{Q}_{ij}\boldsymbol{x} - \mathbf{Q}_{ij}\boldsymbol{x}_i\right) \\ =& -\beta\sum_{j\in\mathcal{N}_i}\left(\boldsymbol{p}_{ij} - \mathbf{Q}_{ij}\boldsymbol{x}\right) + \beta\sum_{j\in\mathcal{N}_i}\mathbf{Q}_{ij}\boldsymbol{e}_i \\ =& -\beta\sum_{j\in\mathcal{N}_i}\left(\tilde{\boldsymbol{p}}_i - \tilde{\boldsymbol{p}}_j\right) + \beta\sum_{j\in\mathcal{N}_i}\mathbf{Q}_{ij}\boldsymbol{e}_i, \end{aligned}$$

which can be rewritten into the following vector form:

$$\dot{\tilde{\boldsymbol{p}}}_f = -\beta\mathcal{L}_{fl}\tilde{\boldsymbol{p}}_l - \beta\mathcal{L}_{ff}\tilde{\boldsymbol{p}}_f + \beta\mathbf{E}\boldsymbol{e},$$

where

$$\mathbf{E} = \mathrm{diag}\left(\textstyle\sum_{j\in\mathcal{N}_{n_l+1}}\mathbf{Q}_{(n_l+1)j}, \ldots, \sum_{j\in\mathcal{N}_n}\mathbf{Q}_{nj}\right).$$

We consider the following Lyapunov function:

$$V_p = \frac{1}{2}\tilde{\boldsymbol{p}}_f^{\mathrm{T}}\tilde{\boldsymbol{p}}_f,$$

whose derivative is

$$\begin{aligned} \dot{V}_p =& \tilde{\boldsymbol{p}}_f^{\mathrm{T}}\dot{\tilde{\boldsymbol{p}}}_f \\ =& -\beta\tilde{\boldsymbol{p}}_f^{\mathrm{T}}\mathcal{L}_{fl}\tilde{\boldsymbol{p}}_l - \beta\tilde{\boldsymbol{p}}_f^{\mathrm{T}}\mathcal{L}_{ff}\tilde{\boldsymbol{p}}_f + \beta\tilde{\boldsymbol{p}}_f^{\mathrm{T}}\mathbf{E}\boldsymbol{e}. \end{aligned}$$

From Theorem 4, it follows the face $\tilde{\boldsymbol{p}}_l \to \boldsymbol{0}$, $\boldsymbol{e} \to \boldsymbol{0}$, $t \to \infty$. Then, $\dot{V}_p \to -\beta\tilde{\boldsymbol{p}}_f^{\mathrm{T}}\mathcal{L}_{ff}\tilde{\boldsymbol{p}}_f$. In view of the fact that the subgraph $\mathcal{G}_f$ is connected from Assumption 3, we can obtain that all eigenvalues of $\mathcal{L}_{ff}$ are positive using the Gerschgorin disk theorem (Horn & Johnson, 2012). Thus, $\mathcal{L}_{ff}$ is positive definite. Therefore, we have $\tilde{\boldsymbol{p}}_f \to \boldsymbol{0}$, $t \to \infty$. ■

5. Simulations

To verify the effectiveness of the proposed formation control methods in Sections 4.1 and 4.2, this section gives simulations to illustrate our results in $\mathbb{R}^2$. We consider 10 agents, 4 of which are leaders, and the remaining 6 agents are followers. (See Box I.)

A nominal configuration lying in $\mathbb{R}^3$ is designed that satisfies Assumption 2. This nominal configuration (See Fig. 2(a) and (b)) is given as: $\boldsymbol{r}_1 = \begin{bmatrix}2 & -2 & 1\end{bmatrix}^T$, $\boldsymbol{r}_2 = \begin{bmatrix}3 & -1 & -1\end{bmatrix}^T$, $\boldsymbol{r}_3 = \begin{bmatrix}3 & 1 & 1\end{bmatrix}^T$, $\boldsymbol{r}_4 = \begin{bmatrix}2 & 2 & -1\end{bmatrix}^T$, $\boldsymbol{r}_5 = \begin{bmatrix}0 & 2 & 1\end{bmatrix}^T$, $\boldsymbol{r}_6 = \begin{bmatrix}0 & -2 & -1\end{bmatrix}^T$, $\boldsymbol{r}_7 = \begin{bmatrix}-3 & -2 & 0\end{bmatrix}^T$, $\boldsymbol{r}_8 = \begin{bmatrix}-3 & 2 & 0\end{bmatrix}^T$, $\boldsymbol{r}_9 = \begin{bmatrix}-3 & 0 & -1\end{bmatrix}^T$, $\boldsymbol{r}_{10} = \begin{bmatrix}-5 & 0 & 1\end{bmatrix}^T$.

We set the augmented linear transformation matrix as

$$\bar{\mathbf{A}} = \begin{cases} \begin{bmatrix} 1 & 0 & 0 & 15 \\ 0 & 1 & 0 & 0 \end{bmatrix} & t \in [\,0,\ 50)\,s \\ \begin{bmatrix} 2\cos 30^\circ & 2\sin 30^\circ & 0 & 30 \\ -2\sin 30^\circ & 2\cos 30^\circ & 0 & 0 \end{bmatrix} & t \in [\,50,\ 100)\,s \\ \begin{bmatrix} -1 & 0.5 & 0 & 34 \\ 0 & 1 & 0 & -10 \end{bmatrix} & t \in [100,\ 150)\,s \\ \begin{bmatrix} 1 & \frac{2}{3} & \frac{4}{3} & 20 \\ 0 & 1 & 1 & -10 \end{bmatrix} & t \in [150,\ 200)\,s \\ \begin{bmatrix} 0 & \frac{8}{3} & \frac{4}{3} & 0 \\ 0 & 0 & -3 & -10 \end{bmatrix} & t \in [200,\ \infty)\,s \end{cases}$$

which is a piecewise function of t, and known by only 4 leaders, i.e., $\mathcal{V}_l = \{1, 2, 3, 4\}$. Agents will first form an initial formation, which is generated by projecting the nominal configuration to the xOy plane. Then, according to the step change of $\bar{\mathbf{A}}$, agents will sequentially perform four linear transformations.

Leaders are employed with the following feedback controller to achieve their desired positions:

$$\boldsymbol{u}_i = -k_l(\boldsymbol{p}_i - \bar{\mathbf{A}}\bar{\boldsymbol{r}}_i), \qquad i \in \mathcal{V}_l \tag{17}$$

where k_l is a positive gain.

5.1. Simulation 1: Stress matrix-based linear formation control

With the nominal configuration, the stress matrix $\boldsymbol{\Omega}$ is computed by using the topology optimization proposed in Xiao et al. (2022) to satisfy Assumption 1. The control parameters for (9) and (17) are selected as $k_l = 3$, $k_f = 10$.

The simulation results are presented in Figs. 3 and 4. Fig. 3 illustrates the changes in the overall formation evolution process. Initially, the group of agents are arranged in a double-column formation at $t = 0$ s. Upon the simulation start, the team of agents rapidly converge to the first desired target formation at $t = 48$ s. Then, with the step changes of $\bar{\mathbf{A}}$, agents sequentially form a new series of target formations. The resulting formations at $t = 98$ s and $t = 148$ s can be transformed by scaling, rotation, shearing, flipping and their combinations from the formation at $t = 48$ s. This means that the proposed linear formation control method has the ability to achieve the transformations that the affine manner can realize. Furthermore, from the results at $t = 198$ s and $t = 248$ s, it is shown that more complex maneuver behaviors can also be achieved by the proposed linear formation control method. It is clear to see that agents 4, 5, and 8 are non-collinear at $t = 198$ s, whereas collinear at $t = 48$ s. This observation leads to the conclusion that this formation variation is not characterized by an affine transformation, but rather by a general linear transformation. Moreover, by utilizing the proposed linear formation control method, new collinear relationships can also be constructed. As it can be seen from the formation shape at $t = 248$ s, agents 2, 4, 6, and 9 are collinear,

$$\Omega = \begin{bmatrix} 1.4900 & -0.5269 & -1.2240 & 1.1241 & -0.2619 & -0.5932 & -0.1954 & 0.1874 & 0 & 0 \\ -0.5269 & 2.3178 & -0.3561 & -1.0728 & 0.3643 & -1.3365 & 0 & 0.1823 & 0 & 0.4276 \\ -1.2240 & -0.3561 & 2.5230 & -0.7408 & -1.3949 & 0.3358 & 0.1918 & 0 & 0.6654 & 0 \\ 1.1241 & -1.0728 & -0.7408 & 1.3043 & -0.3552 & -0.0650 & 0 & -0.0560 & -0.1385 & 0 \\ -0.2619 & 0.3643 & -1.3949 & -0.3552 & 2.4248 & 0.4777 & 0 & -0.9740 & 0 & -0.2810 \\ -0.5932 & -1.3365 & 0.3358 & -0.0650 & 0.4777 & 2.7812 & -0.9306 & 0.0085 & -0.9187 & 0.2408 \\ -0.1954 & 0 & 0.1918 & 0 & 0 & -0.9306 & 1.9232 & 0.7013 & -0.3817 & -1.3087 \\ 0.1874 & 0.1823 & 0 & -0.0560 & -0.9740 & 0.0085 & 0.7013 & 2.0185 & -1.4947 & -0.5731 \\ 0 & 0 & 0.6654 & -0.1385 & 0 & -0.9187 & -0.3817 & -1.4947 & 1.9952 & 0.2726 \\ 0 & 0.4276 & 0 & 0 & -0.2810 & 0.2408 & -1.3087 & -0.5731 & 0.2726 & 1.2220 \end{bmatrix}$$

Box I.

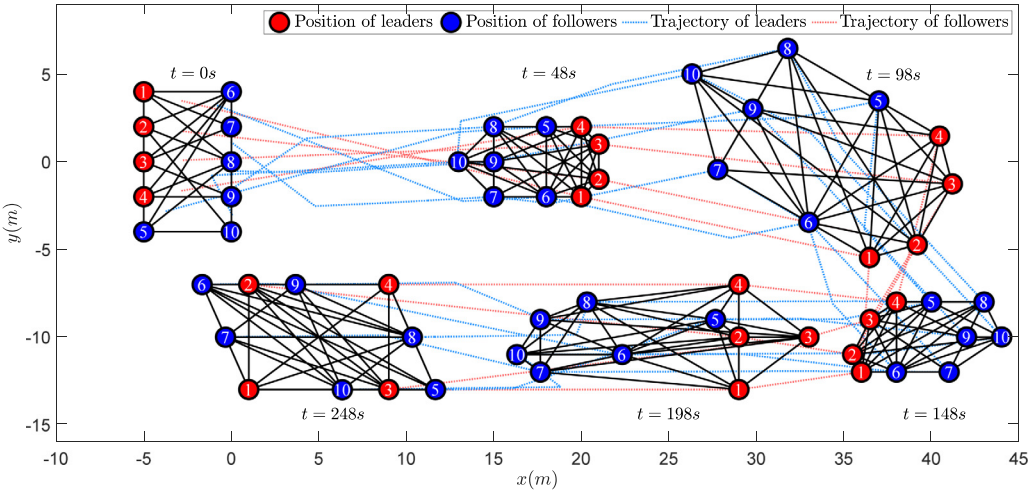

Fig. 3. Trajectories of agents in simulation 1.

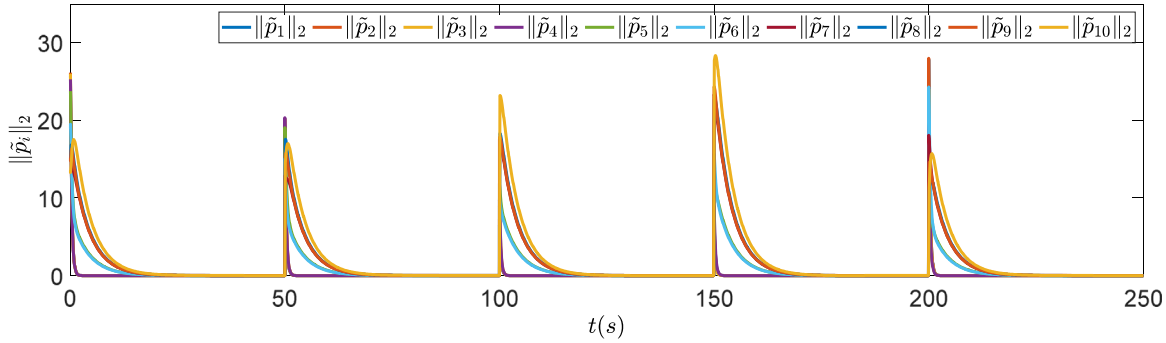

Fig. 4. Position tracking errors in simulation 1.

whereas they are always non-collinear in any other formations in Fig. 3.

Fig. 4 illustrates the position tracking errors of agents. It is clear to see that the position tracking errors converge to zero after every step change of $\bar{\mathbf{A}}$, which implies the effectiveness of the proposed stress matrix-based linear formation tracking control laws (17) and (9).

5.2. Simulation 2: Estimation-based linear formation control

The communication topology among followers is shown in Fig. 2(c) satisfying Assumption 3 for connectivity. Displacements associated with edges $(3, 4)$, $(1, 2)$, and $(1, 3)$ are measurable by followers 5, 6, and 7, respectively. This guarantees Assumption 4, because we can verify that $\{\bar{\mathbf{r}}_{34}, \bar{\mathbf{r}}_{12}, \bar{\mathbf{r}}_{13}\}$ linearly span $\mathbb{R}^3$. The control parameters for (17), (11), (12), and (13) are selected as $k_l = 7$, $\alpha_1 = \alpha_2 = 7$, $\beta = 7$.

The results of the simulation are presented in Figs. 5–7. Similar to simulation 1, Fig. 5 demonstrates that the team of agents can also sequentially achieve the desired target formations by employing the estimation-based linear formation control laws (11)–(13). However, as observed in Fig. 6, following each step change of $\bar{\mathbf{A}}$, the error initially increases before subsequently decreasing. This behavior arises because the estimators need time to re-estimate the new linear formation parameters. The precise

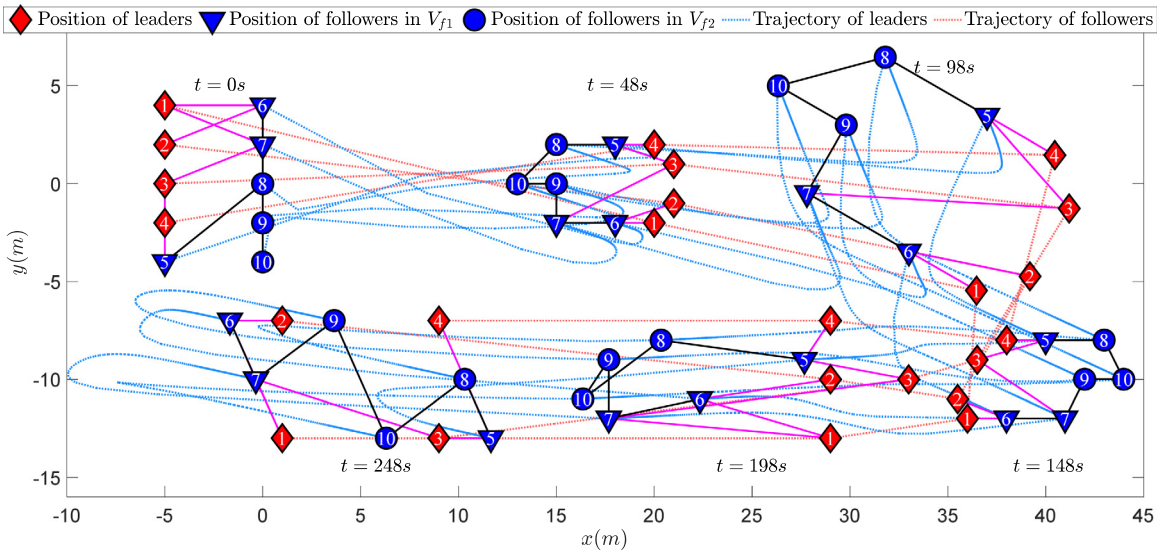

Fig. 5. Trajectories of agents in simulation 2.

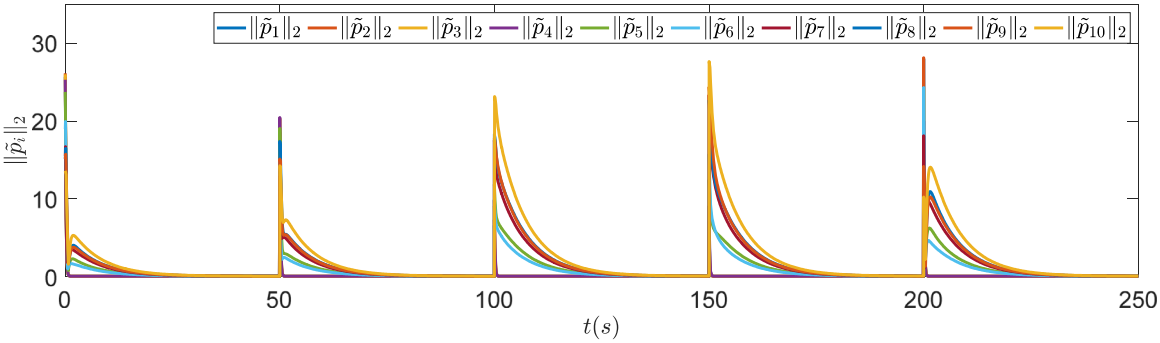

Fig. 6. Position tracking errors in simulation 2.

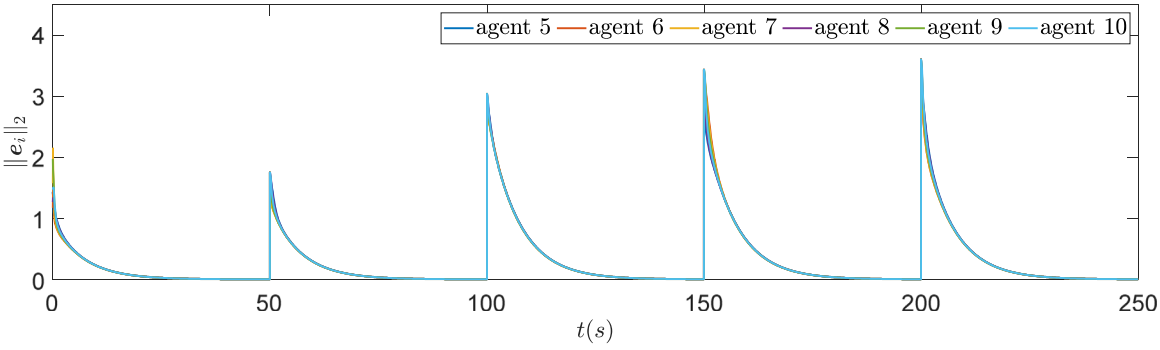

Fig. 7. Estimation errors in simulation 2.

estimation performance of the proposed estimators is shown in Fig. 7, which ensures the convergence of position tracking errors.

6. Conclusion

We have proposed the linear formation control architecture for multi-agent systems. This method requires a pre-defined nominal configuration, whose dimension can be higher than agents' coordinates. We propose two kinds of distributed formation control methods with and without the stress matrix, respectively.

The first method is the stress matrix-based linear formation control scheme, representing an extension of the existing affine formation control approach. When the stress matrix is unavailable, we have proposed the estimation-based linear formation control method, which relies on the measurements of leaders' edges. The estimation-based method only requires a connected graph. Therefore, the utilized topological graph can be sparser than that in the stress matrix-based method, but distributed communication with local estimations is required.

In the future, there will be several important research topics, such as distributed computing of stress matrix, nonlinear formation transformation, and distributed linear formation parameters decision. It is also meaningful to find an efficient stress matrix computation method for large-scale formation.

Acknowledgments

This work was supported in part by the NSFC under grant 62373048, in part by the National Key Research and Development Program of China under No. 2022YFB4702000, No. 2022YFA1004703, in part by the NSFC under Grants 62133002, U1913602, 62088101, in part by the Fundamental Research Funds for the Central Universities and in part by the Shanghai Municipal Science and Technology Major Project (2021SHZDZX0100).

Appendix A. Proof of Lemma 1

In view of the relationship $\mathbf{X}\boldsymbol{z}_i = \left(\boldsymbol{z}_i^{\mathrm{T}} \otimes \mathbf{I}_r\right) \mathrm{vec}\left(\mathbf{X}\right)$, it is considered

$$\left(\mathbf{I}_m \otimes \mathbf{X}\right) \boldsymbol{z} = \begin{bmatrix} \mathbf{X}\boldsymbol{z}_1 \\ \vdots \\ \mathbf{X}\boldsymbol{z}_m \end{bmatrix} = \begin{bmatrix} \left(\boldsymbol{z}_1^{\mathrm{T}} \otimes \mathbf{I}_r\right) \mathrm{vec}\left(\mathbf{X}\right) \\ \vdots \\ \left(\boldsymbol{z}_m^{\mathrm{T}} \otimes \mathbf{I}_r\right) \mathrm{vec}\left(\mathbf{X}\right) \end{bmatrix} = \left(\mathbf{Z} \otimes \mathbf{I}_r\right) \mathrm{vec}\left(\mathbf{X}\right).$$

The proof is completed.

Appendix B. Proof of Lemma 2

B.1. Proof of equivalence of (1) and (2):

According to Section 2.3.2, $\{\bar{\boldsymbol{r}}_i\}_{i=1}^n$ linearly span $\mathbb{R}^{f+1}$ if and only if there exist $f+1$ vectors that are linearly independent, which implies $\mathrm{rank}(\bar{\mathbf{R}}) = f+1$ and $n > f+1$.

B.2. Proof of equivalence of (1) and (3):

It is considered the series of $d(f+1)$ matrices $\left\{\mathbf{E}_{ij}\right\}$, where $\mathbf{E}_{ij} \in \mathbb{R}^{d\times(f+1)}$ ($i = 1,\ldots,d$ and $j = 1,\ldots,f+1$). Only the (i,j)th entry of $\mathbf{E}_{ij}$ is 1 and others are 0. Then, we can construct the following $d(f+1)$ vectors:

$$\left\{\left(\mathbf{I}_n \otimes \mathbf{E}_{ij}\right) \bar{\boldsymbol{r}}\right\}_{i=1,\ldots,d;\ j=1,\ldots,f+1} \tag{18}$$

It is clear that $\mathcal{T}(\bar{\boldsymbol{r}}) = \left\{(\mathbf{I}_n \otimes \bar{\mathbf{A}})\bar{\boldsymbol{r}}, \bar{\mathbf{A}} \in \mathbb{R}^{d\times(f+1)}\right\}$ is the linear span of those vectors in (18). Therefore, $\dim(\mathcal{T}(\bar{\boldsymbol{r}}))$ is equal to the number of linearly independent vectors in (18).

Now we derive the number of linearly independent vectors in (18). It is considered the set of coefficients $\theta_{ij} \in \mathbb{R}$ that satisfy

$$\sum_{i=1}^{d}\sum_{j=1}^{f+1} \theta_{ij} \left(\mathbf{I}_n \otimes \mathbf{E}_{ij}\right) \bar{\boldsymbol{r}} = \boldsymbol{0}_{nd}. \tag{19}$$

According to Lemma 1, we can rewrite (19) in the following form,

$$\sum_{i=1}^{d}\sum_{j=1}^{f+1} \theta_{ij} \left(\bar{\mathbf{R}} \otimes \mathbf{I}_d\right) \mathrm{vec}\left(\mathbf{E}_{ij}\right) = \boldsymbol{0}_{nd}. \tag{20}$$

Eq. (20) admits the following system of linear equations, i.e.,

$$\left(\bar{\mathbf{R}} \otimes \mathbf{I}_d\right) \boldsymbol{\theta} = \boldsymbol{0}_{nd}, \tag{21}$$

where $\boldsymbol{\theta} = \mathrm{vec}\left(\boldsymbol{\Theta}\right) \in \mathbb{R}^{d(f+1)}$, $\left[\boldsymbol{\Theta}\right]_{ij} = \theta_{ij}$.

First, we study the sufficiency of (1) for (3). From the equivalence of (1) and (2), if $\{\bar{\boldsymbol{r}}_i\}_{i=1}^n$ linearly span $\mathbb{R}^f$, it has

$$\mathrm{rank}\left(\bar{\mathbf{R}} \otimes \mathbf{I}_d\right) = \mathrm{rank}\left(\begin{bmatrix}\left(\bar{\mathbf{R}} \otimes \mathbf{I}_d\right) & \boldsymbol{0}_{nd}\end{bmatrix}\right) = d\left(f+1\right).$$

In view of Section 2.5, we know that (21) has the unique solution, i.e., $\boldsymbol{\theta} = \boldsymbol{0}_{d(f+1)}$, which means vectors in (18) are also linearly independent. As a result, we can obtain $\dim(\mathcal{T}(\bar{\boldsymbol{r}})) = d(f+1)$.

Second, we consider the necessity of (1) for (3). From the equivalence of (1) and (2), if $\{\bar{\boldsymbol{r}}_i\}_{i=1}^n$ do not linearly span $\mathbb{R}^f$, it has

$$\mathrm{rank}\left(\bar{\mathbf{R}} \otimes \mathbf{I}_d\right) = \mathrm{rank}\left(\begin{bmatrix}\left(\bar{\mathbf{R}} \otimes \mathbf{I}_d\right) & \boldsymbol{0}_{nd}\end{bmatrix}\right) < d\left(f+1\right).$$

According to Section 2.5, we know that (21) has infinite solutions. There must exist nonzero solutions in terms of $\boldsymbol{\theta}$. Consequently, vectors in (18) are also linearly dependent, which means $\dim(\mathcal{T}(\bar{\boldsymbol{r}})) < d(f+1)$.

B.3. Proof of equivalence between (1) and (4) under Assumption 1:

Since $\boldsymbol{\Omega}$ is the stress matrix of the framework $(\mathcal{G}, \bar{\boldsymbol{r}})$, it has

$$\sum_{j\in\mathcal{N}_i} \omega_{ij}(\bar{\boldsymbol{r}}_i - \bar{\boldsymbol{r}}_j) = \boldsymbol{0}_{f+1}, \qquad i = 1,\ldots,n. \tag{22}$$

By multiplying the linear transformation matrix $\bar{\mathbf{A}}$ on both sides of (22), it gives

$$\sum_{j\in\mathcal{N}_i} \omega_{ij}(\bar{\mathbf{A}}\bar{\boldsymbol{r}}_i - \bar{\mathbf{A}}\bar{\boldsymbol{r}}_j) = \boldsymbol{0}_d, \qquad i = 1,\ldots,n, \tag{23}$$

which implies $\mathcal{T}(\bar{\boldsymbol{r}}) \subseteq \mathrm{null}(\boldsymbol{\Omega} \otimes \mathbf{I}_d)$.

According to Assumption 1, we know $\dim\left(\mathrm{null}\left(\boldsymbol{\Omega} \otimes \mathbf{I}_d\right)\right) = d(f+1)$. In view of the equivalence of (1) and (3), we also know $\dim(\mathcal{T}(\bar{\boldsymbol{r}})) = d(f+1)$. Thus, it is concluded $\mathcal{T}(\bar{\boldsymbol{r}}) = \mathrm{null}(\boldsymbol{\Omega} \otimes \mathbf{I}_d)$. The proof is completed.

References

Alfakih, A. Y. (2011). On bar frameworks, stress matrices and semidefinite programming. *Mathematical Programming*, *129*(1), 113–128.

Anderson, B. D. O., Yu, B. F. C., & Hendrickx, J. M. (2008). Rigid graph control architectures for autonomous formations. *IEEE Control Systems Magazine*, *28*(6), 48–63.

Artin, E. (1988). *Geometric algebra*. Wiley.

Beard, R. W., McLain, T. W., Nelson, D. B., Kingston, D., & Johanson, D. (2006). Decentralized cooperative aerial surveillance using fixed-wing miniature UAVs. *Proceedings of the IEEE*, *94*(7), 1306–1323.

Buckley, I., & Egerstedt, M. (2021). Infinitesimal shape-similarity for characterization and control of bearing-only multirobot formations. *IEEE Transactions on Robotics*, *37*(6), 1921–1935.

Chen, L., Cao, M., & Li, C. (2021). Angle rigidity and its usage to stabilize multiagent formations in 2-D. *IEEE Transactions on Automatic Control*, *66*(8), 3667–3681.

Chen, L., & Sun, Z. (2023). Globally stabilizing triangularly angle rigid formations. *IEEE Transactions on Automatic Control*, *68*(2), 1169–1175.

Chen, L., Yang, Q., Shi, M., Li, Y., & Feroskhan, M. (2022). Stabilizing angle rigid formations with prescribed orientation and scale. *IEEE Transactions on Industrial Electronics*, *69*(11), 11654–11664.

Connelly, R., & Gortler, S. J. (2015). Iterative universal rigidity. *Discrete & Computational Geometry*, *53*(4), 847–877.

Coogan, S., & Arcak, M. (2012). Scaling the size of a formation using relative position feedback. *Automatica*, *48*(10), 2677–2685.

Fathian, K., Safaoui, S., Summers, T. H., & Gans, N. R. (2021). Robust distributed planar formation control for higher order holonomic and nonholonomic agents. *IEEE Transactions on Robotics*, *37*(1), 185–205.

Gao, K., Liu, Y., Zhou, Y., Zhao, Y., & Huang, P. (2022). Practical fixed-time affine formation for multi-agent systems with time-based generators. *IEEE Transactions on Circuits and Systems II Express Briefs*, *69*(11), 4433–4437.

Garcia de Marina, H. (2021). Distributed formation maneuver control by manipulating the complex Laplacian. *Automatica*, *132*, Article 109813.

Garcia de Marina, H., Cao, M., & Jayawardhana, B. (2015). Controlling rigid formations of mobile agents under inconsistent measurements. *IEEE Transactions on Robotics*, *31*(1), 31–39.

Garcia De Marina, H., Jayawardhana, B., & Cao, M. (2016). Distributed rotational and translational maneuvering of rigid formations and their applications. *IEEE Transactions on Robotics*, *32*(3), 684–697.

Gill, E., Sundaramoorthy, P., Bouwmeester, J., Zandbergen, B., & Reinhard, R. (2013). Formation flying within a constellation of nano-satellites: The QB50 mission. *Acta Astronautica*, *82*(1), 110–117.

Godsil, C., & Royle, G. (2001). *Algebraic graph theory*.

Guillet, A., Lenain, R., Thuilot, B., & Rousseau, V. (2017). Formation control of agricultural mobile robots: A bidirectional weighted constraints approach. *Journal of Field Robotics*, *34*(7), 1260–1274.

Han, Z., Wang, L., Lin, Z., & Zheng, R. (2016). Formation control with size scaling via a complex Laplacian-based approach. *IEEE Transactions on Cybernetics*, *46*(10), 2348–2359.

Horn, R. A., & Johnson, C. R. (2012). *Matrix analysis* (2nd ed.).

Lay, D. C., Lay, S. R., & McDonald, J. J. (2014). *Linear algebra and its applications* (5th ed.).

Lee, B. H., & Ahn, H. S. (2016). Distributed formation control via global orientation estimation. *Automatica*, *73*, 125–129.

Li, B., Wang, X., & Wang, Y. (2010). The pseudo-affine transformations in $\mathbb{R}^2$. *Science China. Mathematics*, *53*(3), 755–762.

Lin, Y., Lin, Z., Sun, Z., & Anderson, B. D. O. (2022). A unified approach for finite-time global stabilization of affine, rigid, and translational formation. *IEEE Transactions on Automatic Control*, *67*(4), 1869–1881.

Lin, Z., Wang, L., Chen, Z., Fu, M., & Han, Z. (2016). Necessary and sufficient graphical conditions for affine formation control. *IEEE Transactions on Automatic Control*, *61*(10), 2877–2891.

Liu, Y., Ma, Z., Zhang, F., & Huang, P. (2023). Time-varying formation planning and scaling control for tethered space net robot. *IEEE Transactions on Aerospace and Electronic Systems*, *59*(5), 6717–6728.

Lu, Y., Wen, C., Shen, T., & Zhang, W. (2021). Bearing-based adaptive neural formation scaling control for autonomous surface vehicles with uncertainties and input saturation. *IEEE Transactions on Neural Networks and Learning Systems*, *32*(10), 4653–4664.

Mehdifar, F., Bechlioulis, C. P., Hendrickx, J. M., & Dimarogonas, D. V. (2023). 2-D directed formation control based on bipolar coordinates. *IEEE Transactions on Automatic Control*, *68*(7), 4175–4190.

Motoyama, T., & Cai, K. (2019). Top-down synthesis of multiagent formation control: An eigenstructure assignment based approach. *IEEE Transactions Control of Network Systems*, *6*(4), 1404–1414.

Oba, R., & ichi Tanigawa, S. (2021). Characterizing the universal rigidity of generic tensegrities. *Mathematical Programming*, 1–18.

Onuoha, O., Tnunay, H., Li, Z., & Ding, Z. (2019). Affine formation algorithms and implementation based on triple-integrator dynamics. *Unmanned Systems*, *07*(01), 33–45.

Onuoha, O., Tnunay, H., Wang, C., & Ding, Z. (2020). Fully distributed affine formation control of general linear systems with uncertainty. *Journal of the Franklin Institute*, *357*(17), 12143–12162.

Opsahl, T., & Panzarasa, P. (2009). Clustering in weighted networks. *Social Networks*, *31*(2), 155–163.

Tofallis, C., Gass, S. I., & Harris, C. M. (2013). *Encyclopedia of operations research and management science*. MA: Springer US.

Wang, J., Ding, X., Wang, C., Liang, L., & Hu, H. (2021). Affine formation control for multi-agent systems with prescribed convergence time. *Journal of the Franklin Institute*, *358*(14), 7055–7072.

Wang, J., Ding, X., Wang, C., Zuo, Z., & Ding, Z. (2023). Affine formation control of general linear multi-agent systems with delays. *Unmanned Systems*, *11*(02), 123–132.

Whiteley, W. (2004). Rigidity and scene analysis. In *Handbook of discrete and computational geometry* (pp. 1327–1354).

Xiao, F., Yang, Q., Zhao, X., & Fang, H. (2022). A framework for optimized topology design and leader selection in affine formation control. *IEEE Robotics Automation Letters*, *7*(4), 8627–8634.

Xu, Y., Luo, D., Li, D., You, Y., & Duan, H. (2019). Affine formation control for heterogeneous multi-agent systems with directed interaction networks. *Neurocomputing*, *330*, 104–115.

Xu, Y., Zhao, S., Luo, D., & You, Y. (2020). Affine formation maneuver control of high-order multi-agent systems over directed networks. *Automatica*, *118*, Article 109004.

Yang, Q., Cao, M., Sun, Z., Fang, H., & Chen, J. (2018). Formation scaling control using the stress matrix. In *Proc. IEEE 56th annu. conf. decis. control* (pp. 3449–3454).

Yang, Q., Fang, H., Cao, M., & Chen, J. (2022). Planar affine formation stabilization via parameter estimations. *IEEE Transactions on Cybernetics*, *52*(6), 5322–5332.

Yang, Q., Sun, Z., Cao, M., Fang, H., & Chen, J. (2017). Construction of universally rigid tensegrity frameworks and their applications in formation scaling control. In *Proc. chin. control conf.* (pp. 8177–8182).

Yang, Q., Sun, Z., Cao, M., Fang, H., & Chen, J. (2019). Stress-matrix-based formation scaling control. *Automatica*, *101*, 120–127.

Yang, J., Xiao, F., & Chen, T. (2021). Formation tracking of nonholonomic systems on the special euclidean group under fixed and switching topologies: An affine formation strategy. *SIAM Journal on Control and Optimization*, *59*(4), 2850–2874.

Zhang, X., Lv, J., Lu, S., & Yang, Q. (2022). Distributed decision making on scaling size for obstacle avoidance in affine formation control. In *37th youth acad. annu. conf. Chinese assoc. autom.* (pp. 1001–1006).

Zhang, Y., Wang, S., Wang, X., & Tian, X. (2023). Bearing-based formation control for multiple underactuated autonomous surface vehicles with flexible size scaling. *Ocean Engineering*, *267*, Article 113242.

Zhang, X., Yang, Q., Lyu, J., Zhao, X., & Fang, H. (2024). Distributed variation parameter design for dynamic formation maneuvers with bearing constraints. *IEEE Transactions on Automation Science and Engineering*, *21*(3), 3664–3677.

Zhang, X., Zhang, F., & Huang, P. (2024). Formation planning for tethered multirotor UAV cooperative transportation with unknown payload and cable length. *IEEE Transactions on Automation Science and Engineering*, *21*(3), 3449–3460.

Zhang, X., Zhang, F., Huang, P., et al. (2021). Self-triggered based coordinate control with low communication for tethered multi-UAV collaborative transportation. *IEEE Robotics Automation Letters*, *6*(2), 1559–1566.

Zhao, S. (2018). Affine formation maneuver control of multiagent systems. *IEEE Transactions on Automatic Control*, *63*(12), 4140–4155.

Zhao, S., & Zelazo, D. (2017). Translational and scaling formation maneuver control via a bearing-based approach. *IEEE Transactions Control of Network Systems*, *4*(3), 429–438.

Zhou, B., Huang, B., Mao, L., Zhu, C., & Su, Y. (2022). Distributed observer based event-triggered affine formation maneuver control for underactuated surface vessels with positive minimum inter-event times. *International Journal of Robust and Nonlinear Control*, *32*(14), 7712–77321.

Zhu, C., Huang, B., Lu, Y., Li, X., & Su, Y. (2023). Distributed affine formation maneuver control of autonomous surface vehicles with event-triggered data transmission mechanism. *IEEE Transactions on Control Systems Technology*, *31*(3), 1006–1017.

Xiaozhen Zhang received M.S. degree in navigation, guidance and control, from Northwestern Polytechnical University, Xi'an, China, in 2021. He is currently working toward the Ph.D. degree in control engineering at Beijing Institute of Technology, Beijing, China. His research interests include swarm robotics, multi-agent systems, and distributed control.

Qingkai Yang received the first Ph.D. degree in control science and engineering from the Beijing Institute of Technology, Beijing, China, in 2018, and the second Ph.D. degree in system control from the University of Groningen, Groningen, The Netherlands, in 2018.

He is currently a Professor with the School of Automation, Beijing Institute of Technology. His research interest is in formation control of multi-agent systems and autonomous agents.

Fan Xiao received the M.S. degree in control science and engineering from the Beijing Institute of Technology, Beijing, China, in 2023. She currently works in the Institute of Remote Sensing Satellite, China Aerospace Science and Technology, Beijing, China.

Her research interests include task planning and multi-objective optimization.

Hao Fang received the B.S. degree from the Xi'an University of Technology, Shaanxi, China, in 1995, and the M. S. and Ph.D. degrees from the Xi'an Jiaotong University, Shaanxi, in 1998 and 2002, respectively.

Since 2011, he has been a Professor with the Beijing Institute of Technology, Beijing, China. He held two postdoctoral appointments with the INRIA/France Research Group of COPRIN and the LASMEA (UNR6602 CNRS/Blaise Pascal University, Clermont-Ferrand, France). His research interests include all-terrain mobile robots, robotic control, and multi-agent systems.

Jie Chen received his B.Sc., M.Sc., and the Ph.D. degrees in Control Theory and Control Engineering from the Beijing Institute of Technology, Beijing, China, in 1986, 1996, and 2001, respectively. He was the President of Tongji University, Shanghai, China, during 2018–2023. He is a Professor with the Control Science and Engineering, Beijing Institute of Technology and Tongji University, where he serves as the Director of the National Key Laboratory of Autonomous Intelligent Unmanned Systems (KAIUS).

His research interests include complex systems, multi-agent systems, multi-objective optimization and decision, and constrained nonlinear control. Prof. Chen is currently the Editor-in-Chief of Unmanned Systems and the Journal of Systems Science and Complexity. He has served on the editorial boards of several journals, including the IEEE Transactions on Cybernetics, International Journal of Robust and Nonlinear Control, and Science China Information Sciences. He is a Fellow of IEEE, IFAC, and a member of the Chinese Academy of Engineering.